



HAL
open science

Emergence and global spread of *Listeria monocytogenes* main clinical clonal complex

Alexandra Moura, Noémie Lefrancq, Alexandre Leclercq, Thierry Wirth,
Vítor Borges, Brent Gilpin, Timothy J. Dallman, Joachim Frey, Eelco Franz,
Eva M. Nielsen, et al.

► To cite this version:

Alexandra Moura, Noémie Lefrancq, Alexandre Leclercq, Thierry Wirth, Vítor Borges, et al.. Emergence and global spread of *Listeria monocytogenes* main clinical clonal complex. 2020. pasteur-03696138v1

HAL Id: pasteur-03696138

<https://pasteur.hal.science/pasteur-03696138v1>

Preprint submitted on 10 Jun 2021 (v1), last revised 15 Jun 2022 (v2)

HAL is a multi-disciplinary open access archive for the deposit and dissemination of scientific research documents, whether they are published or not. The documents may come from teaching and research institutions in France or abroad, or from public or private research centers.

L'archive ouverte pluridisciplinaire **HAL**, est destinée au dépôt et à la diffusion de documents scientifiques de niveau recherche, publiés ou non, émanant des établissements d'enseignement et de recherche français ou étrangers, des laboratoires publics ou privés.

Copyright

1 **Emergence and global spread of *Listeria monocytogenes* main clinical clonal complex**

2

3 Alexandra Moura^{1,2,3,*}, Noémie Lefrancq^{4,†}, Alexandre Leclercq^{1,2}, Thierry Wirth^{5,6}, Vítor Borges⁷,
4 Brent Gilpin⁸, Timothy J. Dallman⁹, Joachim Frey¹⁰, Eelco Franz¹¹, Eva M. Nielsen¹², Juno Thomas¹³,
5 Arthur Pightling¹⁴, Benjamin P. Howden¹⁵, Cheryl L. Tarr¹⁶, Peter Gerner-Smidt¹⁶, Simon
6 Cauchemez⁴, Henrik Salje^{4,†,#}, Sylvain Brisse^{17,#}, Marc Lecuit^{1,2,3,18,#,*} for the *Listeria* CC1 Study
7 Group

8

9 ¹ Institut Pasteur, Biology of Infection Unit, Paris, France

10 ² Institut Pasteur, French National Reference Centre and WHO Collaborating Centre *Listeria*, Paris, France

11 ³ Inserm U1117, Paris, France

12 ⁴ Institut Pasteur, Mathematical Modelling of Infectious Diseases Unit, UMR2000, CNRS, Paris, France.

13 ⁵ Institut Systématique Evolution Biodiversité (ISYEB), Museum National d'Histoire Naturelle, CNRS,
14 Sorbonne Université, Université des Antilles, EPHE, Paris, France

15 ⁶ PSL University, EPHE, Paris, France

16 ⁷ National Institute of Health Dr. Ricardo Jorge, Department of Infectious Diseases, Lisbon, Portugal

17 ⁸ Institute of Environmental Science and Research Limited, Christchurch Science Centre, Christchurch,
18 New Zealand

19 ⁹ Public Health England, London, UK

20 ¹⁰ Vetsuisse, University of Bern, Bern, Switzerland

21 ¹¹ National Institute for Public Health and the Environment (RIVM), Centre for Infectious Disease Control,
22 Bilthoven, Netherland

23 ¹² Statens Serum Institut, Copenhagen, Denmark

24 ¹³ National Institute for Communicable Diseases, Division of the National Health Laboratory Service,
25 Johannesburg, South Africa

26 ¹⁴ Biostatistics and Bioinformatics, Center for Food Safety and Applied Nutrition, U.S. Food and Drug
27 Administration, College Park, Maryland, United States

28 ¹⁵ Microbiological Diagnostic Unit Public Health Laboratory, Department of Microbiology and
29 Immunology, The Doherty Institute for Infection and Immunity, University of Melbourne, Victoria,
30 Australia; Infectious Diseases Department, Austin Health, Heidelberg, Victoria, Australia

31 ¹⁶ Centers for Disease Control and Prevention, Atlanta, Georgia, United States

32 ¹⁷ Institut Pasteur, Biodiversity and Epidemiology of Bacterial Pathogens Unit, Paris, France

33 ¹⁸ Université de Paris, Necker-Enfants Malades University Hospital, Division of Infectious Diseases and
34 Tropical Medicine, Institut Imagine, APHP, Paris, France

35

36 † Current address: Department of Genetics, University of Cambridge, Cambridge, UK

37 # Shared senior authorship

38 * Correspondence: amoura@pasteur.fr; marc.lecuit@pasteur.fr

39 **Abstract**

40 Retracing microbial emergence and spread is essential to understanding the evolution and
41 dynamics of pathogens. The bacterial foodborne pathogen *Listeria monocytogenes* clonal
42 complex 1 (*Lm*-CC1) is the most prevalent clonal group associated with listeriosis, and is
43 strongly associated with cattle and dairy products. Here we analysed 2,021 *Lm*-CC1
44 isolates collected from 40 countries, since the first *Lm* isolation to the present day, to
45 define its evolutionary history and population dynamics. Our results suggest that *Lm*-CC1
46 spread worldwide from North America following the Industrial Revolution through two
47 waves of expansion, coinciding with the transatlantic livestock trade in the second half of
48 the 19th century and the rapid growth of cattle farming in the 20th century. *Lm*-CC1 then
49 firmly established at a local level, with limited inter-country spread. This study provides
50 an unprecedented insight into *Lm*-CC1 phylogeography and dynamics and can contribute
51 to effective disease surveillance to reduce the burden of listeriosis.

52 *Listeria monocytogenes* (*Lm*) is a foodborne bacterial zoonotic pathogen that can
53 cause listeriosis, a severe infection with a high case-fatality rate in immunocompromised
54 individuals^{1,2}. Molecular studies have shown the clonal population structure of *Lm*^{3,4} and
55 the worldwide distribution of clonal complex 1 (*Lm*-CC1, initially called epidemic clone
56 ECI^{5,6}), a serotype 4b cosmopolitan clonal group defined by multilocus sequence typing
57 (MLST), which was first isolated from an Italian soldier with meningitis during the first
58 world war (WWI)^{7,8}. Interestingly, *Lm*-CC1 has been reported as the most prevalent
59 clinical clonal complex in several countries⁹⁻¹⁴, and data collected on NCBI Sequence
60 Read Archive also support this conclusion (**Supplementary Figure S1**).

61 While there is no inter-human transmission of listeriosis, it was only in the mid
62 1980's that the foodborne origin of human listeriosis was formally proven¹⁵. Since then,
63 *Lm*-CC1 has been reported in different food matrixes, including dairy products¹⁶⁻¹⁸ which
64 can be heavily contaminated¹⁹ and constitute a major source of human listeriosis^{20,21}.
65 Previous studies have also demonstrated the hypervirulence of *Lm*-CC1⁹, and its higher
66 efficiency in gut colonization and fecal shedding, compared to hypovirulent *Lm*
67 clones^{16,17,22,23}. Moreover, increasing evidence suggests that cattle, which are frequent *Lm*
68 asymptomatic carriers²⁴⁻²⁸ and contribute to *Lm* enrichment in soils²⁵, may constitute a
69 reservoir for *Lm*-CC1. In addition to *Lm* subclinical infections that may contaminate
70 milk^{23,26}, the long-term persistence of *Lm* in cattle manure-amended soils²⁹ also poses
71 serious risks of transmission to fresh produce.

72 Understanding the global evolution of *Lm*-CC1, which is now spread over all
73 continents⁶, as well as its emergence and dissemination across different spatial levels is
74 critical to understand *Lm* population dynamics and to develop better control strategies,
75 especially in countries with ageing and/or immunosuppressed populations who are most
76 at risk for severe infection. However the complex movement of livestock and food

77 products associated with asymptomatic intestinal colonization complicates traditional
78 epidemiological investigations aimed to decipher *Lm* epidemiology by linking isolates in
79 space and time.

80 Here we took a population biology approach to fill this knowledge gap and
81 conducted the largest genomic *Lm*-CC1 study to date, combining genomic and
82 evolutionary approaches to decipher its evolutionary history and pattern of emergence
83 and spread.

84

85 **Results**

86 ***Lm*-CC1 is composed of 3 sublineages of uneven prevalence.** We analyzed 2,021
87 genomes, including 1,230 newly sequenced isolates, originating from 40 countries in 6
88 continents and diverse sources (**Figure 1a**; **Supplementary Table S1**). We covered a
89 time span of 98 years, from the first *Lm* isolation to the present time (1921-2018), and
90 included all contemporary clinical isolates collected between 2012 and mid-2017 within
91 the surveillance framework of 7 countries over 3 continents (**Figure 1a,b**).

92 *Lm*-CC1 genome sizes ranged from 2.77 to 3.25 Mbp, with an average number of
93 2,879±77 coding sequences and G+C content of 37.7-38.3% (**Supplementary Figure**
94 **S2**). On the basis of MLST⁴, 58 sequence types (STs) could be distinguished, with ST1
95 representing 91% ($n=1838$) of isolates. On the basis of core genome MLST (cgMLST)³⁰,
96 we identified within *Lm*-CC1 867 cgMLST types, 92% of which were country-specific
97 (**Supplementary Figure S3**). Rarefaction analysis based on cgMLST resampling did not
98 reach an asymptote (**Supplementary Figure S3**), indicating that despite the high number
99 of sequences obtained in this study, a significant amount of *Lm*-CC1 diversity remains
100 undetected.

101 To better understand the phylogenetic diversity of *Lm*-CC1, we built maximum
102 likelihood phylogenies and identified 3 sublineages (SL1, SL404 and SL150, named
103 based on their smallest ST number). These sublineages have highly uneven frequency
104 (**Figure 1c,d; Supplementary Figure S4**), with SL1 ($n=2002$, isolated worldwide)
105 representing 99.1% of the isolates, while 0.1% are SL404 ($n=2$, found in Europe and
106 North America) and 0.8% represent SL150 ($n=17$, found in North America, Africa and
107 Asia). Within SL1, we further identified 8 distinct genetic clades, which we named GC1
108 to GC8 by decreasing prevalence (**Figure 1; Supplementary Figure S4**). The average
109 genetic distance was 1166 ± 134 wgSNPs (and 478 ± 20 cgMLST alleles) between *Lm*-CC1
110 sublineages, and 76 ± 16 wgSNPs (and 40 ± 9 cgMLST alleles) within SL1 clades
111 (**Supplementary Table S2; Supplementary Figure S5**). The finding that SL1 is by far
112 the major sublineage in *Lm*-CC1 is consistent with either its increased virulence and/or
113 transmission or that SL404 and SL150 are restricted to some yet unknown ecological
114 niches. Within SL1, all different genetic clades were well represented, with strong spatial
115 structure: GC1 is the most prevalent clade in Europe (48%, 593/1237), Asia (68%, 17/25)
116 and South America (64%, 14/22); GC2 is the most prevalent clade in North America
117 (29%, 150/512) and Oceania (52%, 84/163), while GC3 is the most prevalent clade in
118 Africa (80%, 43/54) (**Figure 1e; Supplementary Figure S6**).

119

120 **The *Lm*-CC1 pangenome is diverse.** Analysis of *Lm*-CC1 pangenome identified 10,789
121 orthologous coding sequences (BlastP identity cut-off of $\geq 95\%$), 2,649 of which (92% of
122 the average isolate genome content) present in at least 95% of isolates (core genome)
123 (**Supplementary Figure S7**). The accessory genome included 8,140 gene families, of
124 which 2,844 (35%) were unique to one isolate, and was enriched in transcription,
125 replication/repair and cell wall functions, as well as in gene families of unknown function

126 **(Supplementary Figure S7)**. Plasmids were present in 6% (120/2021) of isolates, and
127 were more prevalent in GC7 (83%, **Supplementary Figure S7**). Intact prophages were
128 present in 62% isolates (1263/2021), and were distributed across the breadth of CC1
129 phylogeny, except in SL404 (**Supplementary Figure S7**). In contrast to *Listeria*
130 pathogenic islands LIPI-1³¹ and LIPI-3³² which were present in all isolates, the *Listeria*
131 genomic island LGI2-1³³, previously identified in CC1 isolates encoding resistance to
132 cadmium and arsenic, was present in 14% (277/2021) isolates and only in GC3 (80%,
133 225/283), GC5 (60%, 38/63) and SL150 (82%, 14/17; **Supplementary Figure S7**).
134 Sublineage-specific genes were detected ($n=81$; **Supplementary Tables S3 and S4**) and
135 pangenome-wide association analyses identified 24 genes that are associated with a
136 clinical origin (**Supplementary Table S5**). The impact of these traits on isolates'
137 differential ecology or virulence remains to be studied, yet the presence of human isolates
138 in all sublineages and clades shows that pathogenic isolates are not restricted to a specific
139 *Lm*-CC1 clade.

140

141 **Emergence and worldwide spread of *Lm*-CC1 main sublineage (SL1) occurred in the**
142 **last 200 years.** To understand *Lm*-CC1 evolution and spread, we performed temporal and
143 phylogeographic analyses on a subset of 200 genomes representative of *Lm*-CC1 genetic
144 and geographic diversity using BEAST³⁴, and on the full dated dataset (1,972 *Lm*-CC1
145 genomes) using Treedater³⁵ (**Supplementary Figures S8 and S9**) and PastML³⁶, under
146 an uncorrelated relaxed clock model (see Material and Methods for details). We estimate
147 a core genome substitution rate of 1.95×10^{-7} substitutions/site/year (95% CI: 1.75×10^{-7} -
148 2.15×10^{-7} ; **Supplementary Figure S8**), consistent with previous findings³⁰. We estimate
149 that *Lm*-CC1 originated about 1,800 years ago (date: 197 AD; 95% CI: 860 BC - 1045
150 AD; **Figure 2b**) and infer that its last common ancestor evolved in North America

151 **(Supplementary Figure S10)**, long before European colonization and the introduction of
152 cattle in the Americas at the end of the 15th century³⁷. Even though the low number of
153 genomes available for Asia, Africa and South America could bias this estimation, the
154 estimated origin was also supported by the measures of population variability, which
155 showed higher genetic diversity within North America **(Supplementary Figure S5;**
156 **Supplementary Table S2)**, and by the basal position of North American *Lm*-CC1
157 isolates in the phylogeny **(Figure 2b, Supplementary Figure S10)**. Whether *Bison bison*
158 populations, which are phylogenetically and ecologically related to bovine and dominated
159 North American prairies prior to colonization by the Europeans and their livestock,
160 played a role in its dispersion remains unknown.

161 Demographic analyses performed using the Bayesian Skyline Plot method³⁸
162 **(Figure 2a)** show that *Lm*-CC1 effective population size was stable up to the middle of
163 the 19th century, followed by two waves of expansion: the first in the late 1880s and the
164 second in the 1930s, coinciding with the first and second ages of globalization,
165 respectively. Tajima's D statistic³⁹ also supported a recent CC1 population expansion and
166 SL1 emergence ($D < 0$; **Supplementary Table S2**). SL1 emerged in North America
167 approximately 160 years ago (date: 1859, 95% CI: 1821-1889), thus closely following the
168 start of the Industrial Revolution **(Figure 3)**. The first SL1 introductions into Europe
169 occurred around 1868 (GC6/GC8 ancestor, 95% CI: 1827-1890), 1871 (GC3/GC7
170 ancestor, 95% CI: 1838-1905) and 1889 (GC2, 95% CI: 1852-1909), concomitant with
171 the 1870 North Atlantic Meat trade agreement⁴⁰. Under this agreement, surplus cattle in
172 North America were shipped to Europe, which had experienced severe livestock
173 shortages due to widespread disease outbreaks (contagious bovine pleuropneumonia and
174 foot and mouth disease), leading to an unprecedented man-made 1000-fold increase in
175 cattle movement From North America to Europe⁴¹. Within the same period, intra-

176 continental diversification also took place, likely driven by cattle movements across
177 North America and railway expansion in North America and Europe. The first SL1
178 introductions that occurred in Oceania (1903, GC2) followed the ‘Great Drought’ of
179 1895-1903, which severely affected livestock⁴².

180 In the following decades and after WWI, multiple CC1 introductions continued
181 from North America into Europe (GC1, GC4, GC5 and GC8) and Asia (GC3) and from
182 Europe to Africa (GC3) (**Figure 3a-b**). The rate of intercontinental bacterial movement
183 declined after 1930s (**Figure 3c**), concomitant with the protectionist trade policies that
184 followed the ‘Great Depression’, which led to a sharp reduction of livestock exports from
185 the USA during the first half of the 20th century⁴³. A second wave of SL1 expansion
186 occurred after this period, likely driven by a new increase in intercontinental movements
187 favoured by the industrialization of food production and globalization of the food and
188 cattle trades (**Figures 2a; Supplementary Figure S11**). Other important human
189 pathogens that have a zoonotic reservoir such as *Escherichia coli* O157:H7⁴⁴ and
190 *Campylobacter jejuni* ST61⁴⁵, have been estimated to have most recent common
191 ancestors (MRCA) at similar times and to have undergone population expansions in the
192 context of animal trade or intensive cattle farming, respectively.

193 A stabilization and relative decline of *Lm*-CC1 population is observed after 1984
194 (**Figure 2a**), coincident with the major advances in infectious diseases’ prevention in
195 dairy cattle⁴⁶ and with the relative decrease of the dairy cattle population in Western
196 countries, in particular Europe (**Supplementary Figure S11**). It also coincides with the
197 time when human listeriosis foodborne origin was formally proven¹⁵, which led to the
198 implementation of surveillance programs in North America and Europe⁴⁷⁻⁵⁰, in particular
199 in the dairy sector following cheese and milk related *Lm*-CC1 outbreaks⁵¹. Whether these

200 findings can be observed in other dairy-associated *L. monocytogenes* clonal complexes,
201 such as CC6 (lineage I) or CC37 and CC101 (lineage II)^{17,52} will deserve future studies.

202

203 **Recent SL1 transmission chains are mostly local.** To further analyze more recent strain
204 transmission dynamics, we compared the genetic diversity of SL1 isolates from 2010-
205 2018 ($n=1,266$) across different spatial scales. To avoid oversampling isolates from
206 outbreak investigations, we excluded all non-clinical isolates from confirmed outbreaks
207 ($n=91$ isolates from 19 outbreaks). We find that pairs of isolates present within the same
208 2-year period and the same country are 18.7 times (95% CI: 4.7-190.7) more likely to
209 have their MRCA within the past 5 years than pairs of isolates coming from other intra-
210 continental countries >1,000 km apart (**Figure 4a**). Furthermore, we observe no
211 difference in the probability of having a recent MRCA in isolates coming from nearby
212 intracontinental countries (<1,000km) than from further apart. Isolates coming from
213 different continents are about 100 times less likely to have an MRCA within the past 5
214 years (0.2; 95% CI: 0.01-2.9) than isolates from the same countries (18.7; 95% CI: 4.7-
215 190.7) (**Figure 4a**). This strong local spatial structure persists for very long time periods,
216 with complete mixing of isolates within a continent appearing only after 50 years (**Figure**
217 **4a**). At a finer spatial scale, available for France (“*départements*”, sub-regional
218 administrative division in France, **Supplementary Figure S12**), a strong local spatial
219 structure is also evident, with the proportion of genetically close pairs of clinical cases
220 being higher between isolates coming from the same French department (4.4%, 95%
221 CI: 1%-10.6%) than between isolates coming from different departments (0.2%, 95% CI
222 0.04%-0.5%), with no effect of distance between them (**Figure 4b**). As expected, in
223 densely urban areas with no farming, such as the city of Paris, clinical strains are
224 significantly less likely to share a recent MRCA than in rural areas or other departments

225 (0.0%, 95% CI: 0.0%-4.4% vs. 3.9%, 95% CI: 1.0%-9.5%) (**Figure 4c**). This result is
226 consistent with urban infections being driven by unrelated *Lm* introductions originating
227 from across the country. Spatial dependence between French isolates persists for 20 years
228 (**Supplementary Figure S13**), with on average 20 (1/0.05) different sources of human
229 infection present at any one time per department (**Figure 4b**).

230

231 **Discussion**

232 Understanding pathogen evolutionary history is essential to understand the population
233 dynamics and biodiversity of microbial infectious agents, and for effective disease
234 surveillance. Here, we have shown that *Lm*-CC1 has spread worldwide following the
235 Industrial Revolution, and that genotypes are now firmly established at a local level, with
236 decades-long localized persistence. These results are consistent with the establishment of
237 separate, locally entrenched sources of *Lm*-CC1 with limited flow of bacteria either
238 within or between countries, in line with cgMLST analyses in which 92% of clusters are
239 country-specific.

240 In the absence of inter-human transmission, this observation likely represents
241 persistent infection sources, *i.e.* individual herds and/or production facilities, in which *Lm*
242 can reside for several years^{28,53}. Outbreak investigations performed at local scale,
243 including in farm environments, would therefore likely improve the identification of
244 contaminating sources, which remain unknown in about 80% of clusters of human
245 cases⁵⁴. Identifying and eradicating sources along the food chain, from the farm to the
246 fork, could lead to significant long-term reductions in the transmission of the *Lm*-CC1.

247 The current scarcity of genomes available for Asia, Africa and South America,
248 and from natural and animal reservoirs may overlook other CC1 clades and could have
249 biased our phylogeographic analyses. Nevertheless, this study sheds unprecedented light

250 onto the evolutionary history, epidemiology and population dynamics of *Lm*-CC1. Similar
251 approaches targeting other major globally distributed clonal complexes will allow
252 clarifying their transmission dynamics and uncovering epidemiological specificities of
253 *Lm* clones. Deciphering the dynamics and drivers of *Lm* sublineages across time and
254 space will inform infection control policies and ultimately reduce the burden of listeriosis.

255

256 **Methods**

257 **Bacterial isolates and genome sequencing.** A total of 2,021 high quality *Listeria*
258 *monocytogenes* clonal complex 1 (CC1) genomes collected by this study group ($n=1,230$)
259 and from NCBI repositories ($n=791$, as of 14 March 2018) were analyzed. These were
260 part of an initial dataset of 2,154 CC1 genomes, from which 133 were discarded due to
261 low sequencing coverage ($<40X$ after read trimming, $n=62$) or low assembly quality
262 (>200 contigs and/or $N50<20Kb$, $n=71$)³⁰. The 2,021 isolates originated from human
263 ($n=1,453$; 72%) and animal hosts ($n=44$; 2%), food ($n=387$; 19%), food-processing
264 environments ($n=88$; 4%), feed ($n=11$; 0.5%), natural environments ($n=11$; 0.6%) or
265 from unknown sources ($n=27$; 1%) (**Figure 1; Table S1**). Isolates were sampled in 40
266 countries from 6 continents, between 1921 and 2018 (**Figure 1; Table S1**). Between 2012
267 and mid-2017, exhaustive sampling was obtained for 7 countries in 3 continents in the
268 context of listeriosis national surveillance programs in Australia ($n=75$), Denmark
269 ($n=42$), France ($n=395$), The Netherlands ($n=53$), New Zealand ($n=34$), the United
270 Kingdom ($n=106$) and the United States ($n=317$). Sequencing reads were obtained using
271 Illumina sequencing platforms (Illumina, San Diego, US) and 2x50 bp ($n=110$), 2x75 bp
272 ($n=2$), 2x100 bp ($n=233$), 2x125 bp ($n=9$), 2x150 bp ($n=1,145$), 2x250 bp ($n=351$),
273 2x300 bp ($n=138$) paired-end runs (**Table S1**).

274

275 **Sequence analysis.** Whole genome sequencing reads were available for 1,988 out of
276 2,021 isolates. Reads were trimmed from adapter sequences and non-confident bases
277 using AlienTrimmer v.0.4⁵⁵ (minimum read length of 30 bases and minimum quality
278 Phred score 20, i.e. 99% base call accuracy) and corrected with Musket v.1.1⁵⁶,
279 implemented in fqCleaner v.3.0 (Alexis Criscuolo, Institut Pasteur). FastQC v.0.11.5⁵⁷
280 was used to assess sequence quality before and after trimming. Assemblies were obtained
281 from paired-ended trimmed reads ≥ 75 bp ($n=1,878$ isolates) by using SPAdes v.3.11.0⁵⁸
282 with the automatic *k-mer*, *--only-assembler* and *--careful* options. For paired-ended
283 trimmed reads of 50 bp ($n=111$), assemblies were built using CLC Assembly Cell v.5.0.0
284 (Qiagen, Denmark), with estimated library insert sizes ranging from 50 to 850 bp. Contigs
285 smaller than 500 bp were discarded from both SPAdes and CLC generated assemblies.

286

287 **Pangenome analysis.** Gene prediction and annotation was carried out from the draft
288 assemblies using Prokka v.1.12⁵⁹. Functional classification was carried out with EGGnog-
289 mapper v2⁶⁰ using DIAMOND (Double Index Alignment of Next-generation sequencing
290 Data)⁶¹. The presence of plasmids, intact prophages and *Listeria* genomic regions was
291 inferred from the assemblies using MOB-suite v.2.0.1⁶², PHASTER (<https://phaster.ca/>)⁶³
292 and BIGSdb-*Lm* (<http://bigsdb.pasteur.fr/listeria/>)^{30,64}, respectively. Pangenome analyses
293 were carried out using Roary v.3.12⁶⁵ with an amino acid identity cut-off of 95% and
294 splitting homologous groups containing paralogs into groups of true orthologs. Venn
295 diagrams were obtained using Venny 2.1 (Oliveros, 2007). Pangenome-wide association
296 analyses were performed using treeWAS v.1.0⁶⁶, to control for phylogenetic structure,
297 using a significance threshold of $p < 10^{-5}$.

298

299 ***In silico* molecular typing.** PCR-serogrouping (5 loci)⁶⁷, MLST (7 loci)⁴ and cgMLST
300 (1748 loci)³⁰ profiles were extracted from draft assemblies using the BIGSdb-*Lm*
301 platform (<http://bigsdb.pasteur.fr/listeria/>) as previously described³⁰. Profiles were
302 compared using the single linkage clustering method implemented in BioNumerics v.7.6
303 (Applied-Maths). cgMLST profiles were classified into cgMLST types (CT) and
304 sublineages (SL) using previous defined cut-offs (7 and 150 allelic mismatches,
305 respectively, out of 1748 loci)³⁰. Rarefaction curves were computed with vegan v. 2.5-6⁶⁸
306 R package, estimated with the rarefaction function (Joshua Jacobs,
307 joshuajacobs.org/R/rarefaction) using 100 random samples per point.

308

309 **Phylogenetic analyses.** Core genome multiple sequence alignments were built from the
310 1748 cgMLST loci concatenated sequences³⁰. Briefly, individual allele sequences were
311 translated into amino acids, aligned separately with MUSCLE v.3.8.31⁶⁹ and back-
312 translated into nucleotide sequence alignment. Concatenation of the 1748 loci alignments
313 resulted in a multiple sequence alignment of 1.57 Mb.

314 In parallel, whole genome SNP (wgSNP)-based alignments were built from trimmed
315 reads and NCBI assemblies using the Snippy v.4.1.0 pipeline
316 (<https://github.com/tseemann/snippy>). The closed CC1 genome F2365 (accession no.
317 NC_002973.6), from the 1985 Canadian cheese outbreak⁷⁰ was used as reference in read
318 mapping, resulting in an alignment of 2.29 Mb.

319 Gubbins v.2.2.0⁷¹ was used to detect recombination regions in both core and whole-
320 genome alignments, using default parameters and a minimum of 3 base substitutions
321 required to identify recombination. Alignment regions positive for recombination were
322 then completely removed from the original alignments, resulting in recombination-free
323 core- and whole-genome alignments of 1.29 Mb and 2.28 Mb, respectively. Maximum

324 likelihood phylogenies were obtained from the recombination-purged alignments using
325 IQ-tree v.1.6.7.2⁷² under the determined best-fit nucleotide substitution model
326 (GTR+F+G4⁷³, as determined by ModelFinder⁷⁴) and ultrafast bootstrapping of 1000
327 replicates⁷⁵. Trees were visualized and annotated with ggtree v.1.14.6⁷⁶ and iTol v.4.2⁷⁷.
328 To measure the degree of genetic variation within sublineages, genetic clades and
329 geographic locations, the pairwise allelic and SNP distance matrices were calculated from
330 the cgMLST profiles and multiple sequence alignments, respectively. SNP distances were
331 computed taking into account only the ATGC polymorphic positions, extracted from the
332 alignments using SNP-sites v.2.4.1⁷⁸.
333 The nucleotide diversity and the Tajima's D statistics per alignment were calculated using
334 the R package PopGenome v.2.6.1⁷⁹.

335

336 **Demographic and spatio-temporal analysis.** To infer the population size changes,
337 Bayesian skyline plots were obtained with BEAST v1.10.4³⁴. The coalescent Bayesian
338 skyline model was chosen due to its flexibility to allow a wide range of demographic
339 scenarios, avoiding the biases of pre-specified parametric models in the estimates of
340 demographic history³⁸. Analyses were performed on a random subset of 200 isolates
341 selected out a subset of 422 isolates representative of genomic and geographic diversity
342 of the full dataset (1 isolate per country per cluster of 99% core genome similarity).
343 Sampling times were positively correlated with the genetic divergence ($p < 0.05$, F-
344 Statistic test; Supplementary Figure S6), as observed using TempEst v1.5.1⁸⁰. BEAST
345 estimations were made using the nucleotide evolutionary model GTR+Γ4 and a default
346 gamma prior distribution of 1, under an uncorrelated relaxed clock model, to allow each
347 branch of the phylogenetic tree to have its own evolutionary rate⁸¹. Runs were performed
348 in triplicates, each consisting of MCMC chains of 400 million iterations, with a 25%

349 burn-in. Parameter values were sampled every 10,000 generations. The effective sample
350 size (ESS) values were confirmed to be higher than 200 for all parameters using Tracer
351 v.1.7⁸². The time of the most recent common ancestor (MRCA) and 95% highest posterior
352 densities (95% HPDs) were inferred from the nodes of the maximum clade credibility
353 tree. To assess the significance of the temporal signatures observed, 10 randomized tip
354 date datasets run under the same parameters were used as controls⁸³. To assess the
355 robustness of the population size inference to changes in the dataset, a second non-
356 overlapping subset of 200 genomes obtained from the same representative subset of 422
357 isolates was analyzed using BEAST with the same parameters as described above.
358 Estimations of the effective population size along the years were computed using Tracer
359 v.1.7⁸².

360 Phylogeography analyses were then extended to the 1972 CC1 genomes for which
361 country and year of isolation were available. Time-calibrated phylogenies were inferred
362 from the maximum likelihood core genome trees (obtained with IQ-tree, as described
363 above) using either Bactdating v1.0.1⁸⁴, Treetime v0.5.2⁸⁵ or Treedater v0.3.0³⁵, assuming
364 a relaxed clock model and the estimated substitution rate of $1.954 \times 10^{-7} \pm 2.0152 \times 10^{-8}$
365 substitutions/site/year (obtained with BEAST as described above). Cophenetic
366 correlations between BEAST and the three alternative large-scale dating methods were
367 evaluated and better R^2 coefficient scores were obtained for Treedater (Supplementary
368 Figure S7). For this reason, the latter dated tree was used in further downstream analyses.
369 Ancestral geographic reconstruction was performed with PastML³⁶ using the MPPA
370 method with an F81-like model and estimated ancestral state probabilities were mapped
371 onto the full time-calibrated phylogeny using the R package ape v5.3⁸⁶.

372

373 **SL1 global transmission dynamics.** To infer the transmission dynamics at a recent time
374 scale (Figure 4a and supplementary Figure S12), we focused on the CC1 main sublineage,
375 and we analyzed the genetic similarity of SL1 isolates from 2010-2018 ($n=1,266$) across
376 different temporal and spatial scales, as described before⁸⁷. To avoid oversampling
377 isolates from outbreak investigations, we excluded all non-clinical isolates from
378 confirmed outbreaks ($n=91$ isolates from 19 outbreaks). We computed the probability P_1
379 that a pair of isolates that satisfy a given location criteria that were sampled within two
380 years of each other had a MRCA in a specific range (0-5 years, 5-20 years, 20-50 years,
381 >50 years), relative to the probability P_{ref} that a pair isolates), sampled within two years
382 of each other, had an MRCA within that particular range. The location criteria used were:
383 i) within countries (both isolates come from the same country); ii) between countries
384 ≤ 1000 km (isolates come from distinct countries, separated by less than 1000 km, from
385 the same continent); iii) between countries >1000 km (isolates come from distinct
386 countries, separated by more than 1000 km, from the same continent; used as reference);
387 and iv) between continents (isolates come from distinct continents). Spatial relationships
388 between isolates were calculated using the centroid coordinates of the countries or regions
389 of origin.

390 We estimated these probabilities using:

$$P_1 = \frac{\# \text{ pairs \{MRCA} \in \text{ window \& sampled within 2 years \& given location criteria\}}}{\# \text{ pairs\{sampled within 2 years \& given location criteria\}}}$$

$$P_{ref} = \frac{\# \text{ pairs\{MRCA} \in \text{ window \& sampled within 2 years \& distant countries\}}}{\# \text{ pairs\{sampled within 2 years \& distant countries\}}}$$

391 Finally, the relative risk (RR) was given by:

$$RR = \frac{P_1}{P_{ref}}$$

392 To measure uncertainty, we used a combination of bootstrapping observations and
393 sampling trees from the Treedater v0.3.0 package³⁵ to incorporate both sampling and tree

394 uncertainty. Over repeated resamples, we first selected a random tree and calculate the
395 evolutionary distance separating all pairs of sequences. Then, we resampled all the
396 isolates with replacement and recalculate RR each time. The 95% confidence intervals are
397 the 2.5% and 97.5% quantiles from the resultant distribution from 1000 resampling
398 events.

399

400 **SL1 local transmission dynamics.** To assess the SL1 local transmission dynamics, we
401 used available data from France. We computed the proportion of closely related pairs of
402 French isolates (defined as having a MRCA<5years) as a function of the spatial distance
403 within and between administrative Departments (**Figure 4b**):

$$p(location) = \frac{\# \text{ pairs } \{ \text{MRCA} < 5 \text{ years \& sampled within 2 years \& given location} \}}{\# \text{ pairs} \{ \text{sampled within 2 years \& given location} \}}$$

404 The different location criteria used are: i) within Department: both isolates come from the
405 same Department; ii) between Departments: isolates come from different Departments,
406 separated by a distance from 50 to >500km. The French Departments are shown in the
407 map in **Figure S11**.

408 As shown in Salje et al.⁸⁷, the reciprocal of $p(\textit{within department})$ represents the lower
409 limit of the number of sources of human infection circulating within a Department.

410 To assess uncertainty, we used the bootstrapping approach as described above.

411 To explore possible differences between Departments, we computed the relative risk that
412 a pair of isolates share a MRCA of less than 5 years when both come from the same
413 department compared to when coming from different departments. We looked at 2
414 different groups of departments: i) Paris alone (**Figure 4c, left**): within Paris (both
415 isolates come from Paris) and between Paris and other departments (for each pair of
416 isolates, one of them come from Paris, and the other one from another department); ii)
417 other departments, except Paris (**Figure 4c, right**): with other departments (both isolates

418 come from the same department, excluding Paris) and between all other departments
419 (isolates come from 2 different departments, excluding Paris). For each group, to compute
420 the relative risk RR , we used the same approach as explained above. We estimated:

$$P_1 = \frac{\# \text{ pairs \{MRCA < 5 years \& sampled within 2 years \& same department\}}}{\# \text{ pairs\{sampled within 2 years \& same department\}}}$$
$$P_{\text{ref}} = \frac{\# \text{ pairs\{MRCA < 5 years \& sampled within 2 years \& different departments\}}}{\# \text{ pairs\{sampled within 2 years \& different departments\}}}$$

421 Finally, the relative risk is given by:

$$RR = \frac{P_1}{P_{\text{ref}}}$$

422 To determine uncertainty, we used the same bootstrapping approach as described above.
423 To assess the statistical significance of each RR , we performed a one-tailed test. We set
424 the null hypothesis (H_0) as $RR \leq 1$, and alternative hypothesis (H_1) as $RR > 1$. For each
425 group, composed N bootstrap events, we computed:

$$p = \frac{\sum_{i=1}^N I(RR_i \leq 1)}{N}$$

426

427 **Data availability.** All sequence data will be made available in NCBI-SRA and EBI-ENA
428 public archives upon acceptance.

429

430 **Acknowledgements**

431 The findings and conclusions in this report are those of the authors and do not
432 necessarily represent the official position of the Centers for Disease Control and
433 Prevention. The authors thank all participating laboratories and the PulseNet International
434 Network members for their contributions. The authors are also grateful to Martin
435 Wiedmann, Mark Achtman and Jana Haase for providing cultures of historical isolates, to
436 Thomas Cantinelli and Laure Diancourt for contributions to the initial sequencing of CC1
437 isolates, to Keith Jolley, Youssef Ghorbal and Bryan Brancotte for BIGSdb-*Listeria*
438 maintenance and software updates, to Eduardo Rocha, Etienne Simon-Lorière, Anna
439 Zhukova, Sophie Creno, Eric Deveaud, Guy Bayle and Erik Volz for insightful feedback
440 on methodological issues, and François-Xavier Weill for critical reading. This work used
441 the computational and storage services (TARS cluster) provided by the IT department at
442 Institut Pasteur, Paris.

443

444 **Funding**

445 This study was supported financially by Institut Pasteur, Inserm, Santé Publique
446 France, the European Research Council, the Swiss National Science Foundation (Project
447 SINERGIA, Grant No. CRSII3_147692), the Investissement d’Avenir program
448 Laboratoire d’Excellence ‘Integrative Biology of Emerging Infectious Diseases’ (grant
449 ANR-10-LABX-62-IBEID), and the Advanced Molecular Detection (AMD) initiative at
450 CDC. Marc Lecuit is a member of Institut Universitaire de France.

451

452 **Author contributions**

453 ML coordinated the project. ML and SB conceived and designed the study. AM,
454 NL, TW, SC, HS analysed the data, together with SB and ML. AL, VB, BG, TJD, JF, EF,

455 EMN, JT, AP, BPH, CT, PGS, SB, ML and the *Listeria* CC1 study group obtained the
456 isolates, acquired metadata data collection and genome sequences. AM, HS and ML
457 wrote the manuscript. All authors commented and edited the final version of the
458 manuscript.

459 References

- 460 1. Swaminathan, B. & Gerner-Smidt, P. The epidemiology of human listeriosis. *Microbes*
461 *Infect.* **9**, 1236–1243 (2007).
- 462 2. Charlier, C. *et al.* Clinical features and prognostic factors of listeriosis: the MONALISA
463 national prospective cohort study. *Lancet Infect. Dis.* **17**, 510–519 (2017).
- 464 3. Orsi, R. H., Bakker, H. C. de. & Wiedmann, M. *Listeria monocytogenes* lineages:
465 genomics, evolution, ecology, and phenotypic characteristics. *Int. J. Med. Microbiol.* **301**,
466 79–96 (2011).
- 467 4. Ragon, M. *et al.* A new perspective on *Listeria monocytogenes* evolution. *PLoS Pathog.* **4**,
468 e1000146 (2008).
- 469 5. Cantinelli, T. *et al.* ‘Epidemic clones’ of *Listeria monocytogenes* are widespread and
470 ancient clonal groups. *J. Clin. Microbiol.* **51**, 3770–3779 (2013).
- 471 6. Chenal-Francisque, V. *et al.* Worldwide distribution of major clones of *Listeria*
472 *monocytogenes*. *Emerg. Infect. Dis.* **17**, 1110–1112 (2011).
- 473 7. Dumont, J. & Cotoni, L. Bacille semblable au bacielle du Rouget du porc rencontré dans le
474 liquide céphalo-rachidien d’un méningitique. *Ann. Inst. Pasteur (Paris)*. **35**, 625–633
475 (1921).
- 476 8. Hyden, P. *et al.* Draft genome sequence of a 94-year-old *Listeria monocytogenes* isolate,
477 SLCC208. *Genome Announc.* **4**, e01572-15 (2016).
- 478 9. Maury, M. *et al.* Uncovering *Listeria monocytogenes* hypervirulence by harnessing its
479 biodiversity. *Nat. Genet.* **48**, 308–313 (2016).
- 480 10. Kwong, J. C. *et al.* Prospective whole genome sequencing enhances national surveillance
481 of *Listeria monocytogenes*. *J. Clin. Microbiol.* **54**, JCM.02344-15 (2015).
- 482 11. Bertrand, S. *et al.* Diversity of *Listeria monocytogenes* strains of clinical and food chain
483 origins in Belgium between 1985 and 2014. *PLoS One* **11**, e0164283 (2016).
- 484 12. Toledo, V. *et al.* Genomic diversity of *Listeria monocytogenes* isolated from clinical and
485 non-clinical samples in Chile. *Genes (Basel)*. **9**, 396 (2018).
- 486 13. Hilliard, A. *et al.* Genomic characterization of *Listeria monocytogenes* isolates associated
487 with clinical listeriosis and the food production environment in Ireland. *Genes (Basel)*. **9**,
488 171 (2018).
- 489 14. Scaltriti, E. *et al.* Population Structure of *Listeria monocytogenes* in Emilia-Romagna
490 (Italy) and implications on whole genome sequencing surveillance of listeriosis. *Front.*
491 *Public Heal.* **8**, (2020).
- 492 15. Schlech, W. F. *et al.* Epidemic listeriosis — evidence for transmission by food. *N. Engl. J.*
493 *Med.* **308**, 203–206 (1983).
- 494 16. Maury, M. M. *et al.* Hypervirulent *Listeria monocytogenes* clones’ adaption to mammalian
495 gut accounts for their association with dairy products. *Nat. Commun.* **10**, 2488 (2019).
- 496 17. Painset, A. *et al.* Liseq – Whole-genome sequencing of a cross-sectional survey of *Listeria*
497 *monocytogenes* in ready-to-eat foods and human clinical cases in Europe. *Microb.*
498 *Genomics* **5**, e000257 (2019).
- 499 18. Félix, B. *et al.* Population genetic structure of *Listeria monocytogenes* strains isolated from
500 the pig and pork production chain in France. *Front. Microbiol.* **9**, (2018).
- 501 19. Dalton, C. B. *et al.* An outbreak of gastroenteritis and fever due to *Listeria monocytogenes*
502 in milk. *N. Engl. J. Med.* **336**, 100–5 (1997).
- 503 20. Costard, S., Espejo, L., Groenendaal, H. & Zagmutt, F. J. Outbreak-related disease burden
504 associated with consumption of unpasteurized cow’s milk and cheese, United States,
505 2009–2014. *Emerg. Infect. Dis.* **23**, 957–964 (2017).
- 506 21. Filipello, V. *et al.* Attribution of *Listeria monocytogenes* human infections to food and
507 animal sources in Northern Italy. *Food Microbiol.* **89**, (2020).
- 508 22. Dreyer, M. *et al.* *Listeria monocytogenes* sequence type 1 is predominant in ruminant
509 rhombencephalitis. *Sci. Rep.* **6**, 36419 (2016).
- 510 23. Papić, B., Pate, M., Félix, B. & Kušar, D. Genetic diversity of *Listeria monocytogenes*
511 strains in ruminant abortion and rhombencephalitis cases in comparison with the natural

- environment. *BMC Microbiol.* **19**, 299 (2019).
- 513 24. Garcia-Garcera, M. *et al.* *Listeria monocytogenes* faecal carriage is common and driven by
514 microbiota. *bioRxiv* (2020).
- 515 25. Nightingale, K. K. *et al.* Ecology and transmission of *Listeria monocytogenes* infecting
516 ruminants and in the farm environment. *Appl. Environ. Microbiol.* **70**, 4458–4467 (2004).
- 517 26. Esteban, J. I., Oporto, B., Aduriz, G., Juste, R. A. & Hurtado, A. Faecal shedding and
518 strain diversity of *Listeria monocytogenes* in healthy ruminants and swine in Northern
519 Spain. *BMC Vet. Res.* **5**, (2009).
- 520 27. Lyautey, E. *et al.* Characteristics and frequency of detection of fecal *Listeria*
521 *monocytogenes* shed by livestock, wildlife, and humans. *Can. J. Microbiol.* **53**, 1158–1167
522 (2007).
- 523 28. Borucki, M. K. *et al.* Genetic diversity of *Listeria monocytogenes* strains from a high-
524 prevalence dairy farm. *Appl. Environ. Microbiol.* **71**, 5893–5899 (2005).
- 525 29. Jiang, X., Islam, M., Morgan, J. & Doyle, M. P. Fate of *Listeria monocytogenes* in bovine
526 manure - Amended soil. *J. Food Prot.* **67**, 1676–1681 (2004).
- 527 30. Moura, A. *et al.* Whole genome-based population biology and epidemiological
528 surveillance of *Listeria monocytogenes*. *Nat. Microbiol.* **2**, 16185 (2016).
- 529 31. Kuenne, C. *et al.* Reassessment of the *Listeria monocytogenes* pan-genome reveals
530 dynamic integration hotspots and mobile genetic elements as major components of the
531 accessory genome. *BMC Genomics* **14**, 47 (2013).
- 532 32. Cotter, P. D. *et al.* Listeriolysin S, a novel peptide haemolysin associated with a subset of
533 lineage I *Listeria monocytogenes*. *PLoS Pathog.* **4**, e1000144 (2008).
- 534 33. Lee, S., Ward, T. J., Jima, D. D., Parsons, C. & Kathariou, S. The arsenic
535 resistance-associated *Listeria* genomic island LGI2 exhibits sequence and integration site
536 diversity and a propensity for three *Listeria monocytogenes* clones with enhanced
537 virulence. *Appl. Environ. Microbiol.* **83**, (2017).
- 538 34. Suchard, M. A. *et al.* Bayesian phylogenetic and phylodynamic data integration using
539 BEAST 1.10. *Virus Evol.* **4**, vey016 (2018).
- 540 35. Volz, E. M. & Frost, S. D. W. Scalable relaxed clock phylogenetic dating. *Virus Evol.* **3**,
541 1–9 (2017).
- 542 36. Ishikawa, S. A., Zhukova, A., Iwasaki, W. & Gascuel, O. A fast likelihood method to
543 reconstruct and visualize ancestral scenarios. *Mol. Biol. Evol.* **36**, 2069–2085 (2019).
- 544 37. Bowling, G. A. The introduction of cattle into colonial North America. *J. Dairy Sci.* **25**,
545 129–154 (1942).
- 546 38. Drummond, A. J., Rambaut, A., Shapiro, B. & Pybus, O. G. Bayesian coalescent inference
547 of past population dynamics from molecular sequences. *Mol. Biol. Evol.* **22**, 1185–1192
548 (2005).
- 549 39. Tajima, F. Statistical method for testing the neutral mutation hypothesis by DNA
550 polymorphism. *Genetics* **123**, 585–595 (1989).
- 551 40. World Trade Organization. *World trade report.* (World Trade Organization, 2013).
- 552 41. Zimmerman, W. D. Live cattle export trade between United States and Great Britain,
553 1868-1885. *Agric. Hist.* **36**, 46–52 (1962).
- 554 42. Burroughs, W. J. & World Meteorological Organization. *Climate: into the 21st century.*
555 (Cambridge University Press, 2003).
- 556 43. Groombridge, B. *Global Biodiversity: status of the Earth's living resources.* (Springer
557 Netherlands, 1992).
- 558 44. Franz, E. *et al.* Phylogeographic analysis reveals multiple international transmission events
559 have driven the global emergence of *Escherichia coli* O157:H7. *Clin. Infect. Dis.* **69**, 428–
560 437 (2019).
- 561 45. Mourkas, E. *et al.* Agricultural intensification and the evolution of host specialism in the
562 enteric pathogen *Campylobacter jejuni*. *Proc. Natl. Acad. Sci.* **117**, 11018–11028 (2020).
- 563 46. LeBlanc, S. J., Lissemore, K. D., Kelton, D. F., Duffield, T. F. & Leslie, K. E. Major
564 advances in disease prevention in dairy cattle. *J. Dairy Sci.* **89**, 1267–1279 (2006).
- 565 47. Cartwright, E. J. *et al.* Listeriosis outbreaks and associated food vehicles, United States,
566 1998-2008. *Emerg. Infect. Dis.* **19**, 1–9 (2013).

- 567 48. De Valk, H. *et al.* Two consecutive nationwide outbreaks of listeriosis in France, October
568 1999-February 2000. *Am. J. Epidemiol.* **154**, 944–950 (2001).
- 569 49. Goulet, V. *et al.* Effect of prevention measures on incidence of human listeriosis, France,
570 1987-1997. *Emerg. Infect. Dis.* **7**, 983–989 (2001).
- 571 50. Tappero, J. W., Schuchat, A., Deaver, K. A., Mascola, L. & Wenger, J. D. Reduction in
572 the incidence of human listeriosis in the United States. Effectiveness of prevention efforts?
573 *JAMA* **273**, 1118–22 (1995).
- 574 51. Kathariou, S. Foodborne outbreaks of listeriosis and epidemic-associated lineages of
575 *Listeria monocytogenes*. in *Microbial Food Safety in Animal Agriculture* 243–256
576 (Blackwell Publishing, 2008). doi:10.1002/9780470752616.ch25
- 577 52. Maury, M. M. *et al.* Spontaneous loss of virulence in natural populations of *Listeria*
578 *monocytogenes*. *Infect. Immun.* **85**, 1–13 (2017).
- 579 53. Castro, H., Jaakkonen, A., Hakkinen, M., Korkeala, H. & Lindström, M. Occurrence,
580 persistence, and contamination routes of *Listeria monocytogenes* genotypes on three
581 Finnish dairy cattle farms: A longitudinal study. *Appl. Environ. Microbiol.* **84**, (2018).
- 582 54. Moura, A. *et al.* Real-time whole-genome sequencing for surveillance of *Listeria*
583 *monocytogenes*, France. *Emerg. Infect. Dis.* **23**, 1462–1470 (2017).
- 584 55. Criscuolo, A. & Brisse, S. AlienTrimmer: A tool to quickly and accurately trim off
585 multiple short contaminant sequences from high-throughput sequencing reads. *Genomics*
586 **102**, 500–506 (2013).
- 587 56. Liu, Y., Schröder, J. & Schmidt, B. Musket: A multistage k-mer spectrum-based error
588 corrector for Illumina sequence data. *Bioinformatics* **29**, 308–315 (2013).
- 589 57. Andrews, S. FastQC: a quality control tool for high throughput sequence data. *Available*
590 *online at: <http://www.bioinformatics.babraham.ac.uk/projects/fastqc>* (2010).
- 591 58. Bankevich, A. *et al.* SPAdes: a new genome assembly algorithm and its applications to
592 single-cell sequencing. *J. Comput. Biol.* **19**, 455–477 (2012).
- 593 59. Seemann, T. Prokka: Rapid prokaryotic genome annotation. *Bioinformatics* **30**, 2068–2069
594 (2014).
- 595 60. Huerta-Cepas, J. *et al.* Fast genome-wide functional annotation through orthology
596 assignment by eggNOG-mapper. *Mol. Biol. Evol.* **34**, 2115–2122 (2017).
- 597 61. Buchfink, B., Xie, C. & Huson, D. H. Fast and sensitive protein alignment using
598 DIAMOND. *Nature Methods* **12**, 59–60 (2014).
- 599 62. Robertson, J. & Nash, J. H. E. MOB-suite: software tools for clustering, reconstruction
600 and typing of plasmids from draft assemblies. *Microb. genomics* **4**, (2018).
- 601 63. Arndt, D. *et al.* PHASTER: a better, faster version of the PHAST phage search tool.
602 *Nucleic Acids Res.* **44**, W16--W21 (2016).
- 603 64. Jolley, K. A. & Maiden, M. C. J. BIGSdb: Scalable analysis of bacterial genome variation
604 at the population level. *BMC Bioinformatics* **11**, 595 (2010).
- 605 65. Page, A. J. *et al.* Roary: Rapid large-scale prokaryote pan genome analysis. *Bioinformatics*
606 **31**, 3691–3693 (2015).
- 607 66. Collins, C. & Didelot, X. A phylogenetic method to perform genome-wide association
608 studies in microbes that accounts for population structure and recombination. *PLoS*
609 *Comput. Biol.* **14**, e1005958 (2018).
- 610 67. Doumith, M., Buchrieser, C., Glaser, P., Jacquet, C. & Martin, P. Differentiation of the
611 major *Listeria monocytogenes* serovars by multiplex PCR. *J. Clin. Microbiol.* **42**, 3819–
612 3822 (2004).
- 613 68. Dixon, P. VEGAN, a package of R functions for community ecology. *J. Veg. Sci.* **14**, 927–
614 930 (2003).
- 615 69. Edgar, R. C. MUSCLE: Multiple sequence alignment with high accuracy and high
616 throughput. *Nucleic Acids Res.* **32**, 113 (2004).
- 617 70. Mascola, L. *et al.* Listeriosis: an uncommon opportunistic infection in patients with
618 acquired immunodeficiency syndrome. A report of five cases and a review of the
619 literature. *Am. J. Med.* **84**, 162–164 (1988).
- 620 71. Croucher, N. J. *et al.* Rapid phylogenetic analysis of large samples of recombinant
621 bacterial whole genome sequences using Gubbins. *Nucleic Acids Res.* **43**, e15 (2015).

- 622 72. Nguyen, L. T., Schmidt, H. A., Von Haeseler, A. & Minh, B. Q. IQ-TREE: A fast and
623 effective stochastic algorithm for estimating maximum-likelihood phylogenies. *Mol. Biol.*
624 *Evol.* **32**, 268–274 (2015).
- 625 73. Tavaré, S. Some probabilistic and statistical problems in the analysis of DNA sequences.
626 *American Mathematical Society: Lectures on Mathematics in the Life Sciences* (1986).
627 doi:citeulike-article-id:4801403
- 628 74. Kalyaanamoorthy, S., Minh, B. Q., Wong, T. K. F., Von Haeseler, A. & Jermin, L. S.
629 ModelFinder: Fast model selection for accurate phylogenetic estimates. *Nat. Methods* **14**,
630 587–589 (2017).
- 631 75. Minh, B. Q., Nguyen, M. A. T. & von Haeseler, A. Ultrafast approximation for
632 phylogenetic bootstrap. *Mol. Biol. Evol.* **30**, 1188–1195 (2013).
- 633 76. Yu, G., Smith, D. K., Zhu, H., Guan, Y. & Lam, T. T.-Y. ggtree: an r package for
634 visualization and annotation of phylogenetic trees with their covariates and other
635 associated data. *Methods Ecol. Evol.* **8**, 28–36 (2017).
- 636 77. Letunic, I. & Bork, P. Interactive tree of life (iTOL) v3: an online tool for the display and
637 annotation of phylogenetic and other trees. *Nucleic Acids Res.* **44**, W242–245 (2016).
- 638 78. Page, A. J. *et al.* SNP-sites: rapid efficient extraction of SNPs from multi-FASTA
639 alignments. *Microb. genomics* **2**, e000056 (2016).
- 640 79. Pfeifer, B., Wittelsbürger, U., Ramos-Onsins, S. E. & Lercher, M. J. PopGenome: an
641 efficient Swiss army knife for population genomic analyses in R. *Mol. Biol. Evol.* **31**,
642 1929–1936 (2014).
- 643 80. Rambaut, A., Lam, T. T., Max Carvalho, L. & Pybus, O. G. Exploring the temporal
644 structure of heterochronous sequences using TempEst (formerly Path-O-Gen). *Virus Evol.*
645 **2**, (2016).
- 646 81. Drummond, A. J., Ho, S. Y. W., Phillips, M. J. & Rambaut, A. Relaxed phylogenetics and
647 dating with confidence. *PLoS Biol.* **4**, e88 (2006).
- 648 82. Rambaut, A., Drummond, A. J., Xie, D., Baele, G. & Suchard, M. A. Posterior
649 summarization in Bayesian phylogenetics using Tracer 1.7. *Syst. Biol.* **67**, 901–904 (2018).
- 650 83. Firth, C. *et al.* Using time-structured data to estimate evolutionary rates of double-stranded
651 DNA viruses. *Mol. Biol. Evol.* **27**, 2038–51 (2010).
- 652 84. Didelot, X., Croucher, N. J., Bentley, S. D., Harris, S. R. & Wilson, D. J. Bayesian
653 inference of ancestral dates on bacterial phylogenetic trees. *Nucleic Acids Res.* **46**, e134
654 (2018).
- 655 85. Himmelmann, L. & Metzler, D. TreeTime: an extensible C++ software package for
656 Bayesian phylogeny reconstruction with time-calibration. *Bioinformatics* **25**, 2440–1
657 (2009).
- 658 86. Paradis, E. & Schliep, K. ape 5.0: an environment for modern phylogenetics and
659 evolutionary analyses in R. *Bioinformatics* **35**, 526–528 (2019).
- 660 87. Salje, H. *et al.* Dengue diversity across spatial and temporal scales: Local structure and the
661 effect of host population size. *Science (80-.)*. **355**, 1302–1306 (2017).
662

663 Figure legends

664 **Figure 1. Geographical and temporal distribution of the isolates used in this study (N=2,021)** 665 **and phylogenetic analyses**

666 **a.** Geographical distribution and source distribution. Sampled countries are colored in blue, with
667 hue gradient according to the number of isolates. Pie charts are proportional to the number of
668 isolates sampled in each continent and represent the repartition of sample source types, using the
669 source color key indicated in panel d. Out of 2,021 genomes, 8 isolates had unknown sampling
670 location and are not shown in the map. **b.** Temporal distribution of isolates collected in this study.
671 Darker blue bars indicate the period for which exhaustive clinical sampling was obtained for 7
672 countries spanning 3 continents (2012-2017; US, FR, UK, DK, NL, AU, NZ). **c.** Unrooted
673 maximum-likelihood phylogenetic tree of 2,021 *Lm*-CC1 genomes. The tree was generated from
674 analysis (GTR+F+G4 model, 1000 ultra-fast bootstraps) of a 1.29 Mb recombination-purged core
675 genome alignment. **d.** Midpoint rooted maximum-likelihood phylogenetic tree of 2,002 SL1
676 genomes based on a recombination-purged core genome alignment of 1.29 Mb. The four external
677 rings indicate the world region, year, type of infection and source type, respectively. The two
678 inner rings indicate ST1 isolates and the 8 SL1 genetic clades identified in this study,
679 respectively. **e.** Percentage of genomes per phylogroup and world region. Partitions are colored by
680 world regions (left) and phylogroups (right), using the same color code as in panel d.

681

682 **Figure 2. Bayesian temporal and demographic analyses on a representative 200 isolate** 683 **dataset**

684 **a.** Bayesian skyline plot (BSP) with the estimation of *Lm*-CC1 effective population size (N_e). The
685 y-axis refers to the predicted number of individuals (log scale) and the x-axis to the timescale (in
686 years). The median population size is marked in blue with its 95% high posterior density (HDP)
687 in gray. Blue vertical panels delimitate the three globalization ages (1870-1914, 1944-1971, 1989-
688 present). **b.** Bayesian time-calibrated tree. Nodes represent the estimated mean divergence times
689 and gray bars represent the 95% HPD confidence intervals of node age. Scale indicates time (in
690 years). Terminal branches and tips are colored by continents, as indicated in the key panel.

691

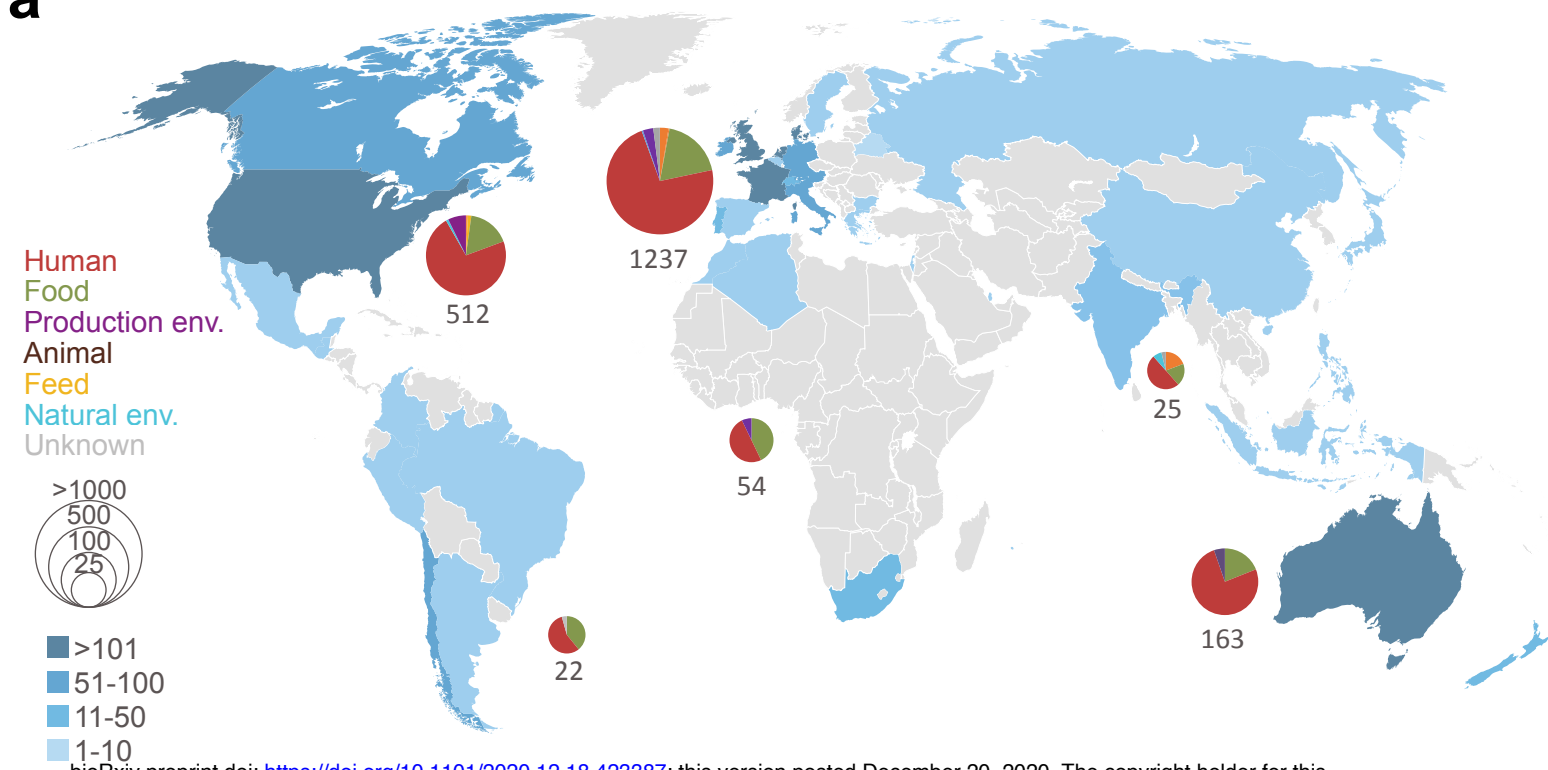
692 **Figure 3. Phylogeography of sublineage SL1**

693 **a.** Time-calibrated phylogeny based on the 1956 SL1 genomes. Pies at the nodes represent the
694 probability of ancestral geographical locations, estimate using PastML using the MPPA method
695 with an F81-like model. **b.** Inferred spread of SL1 populations across continents. The first
696 introductions of each phylogroup are represented by arrows from their estimated world region
697 origin. **c.** Proportion of inter-continental transitions per 10-year bins, normalized by the total
698 number of phylogenetic branches per bin.

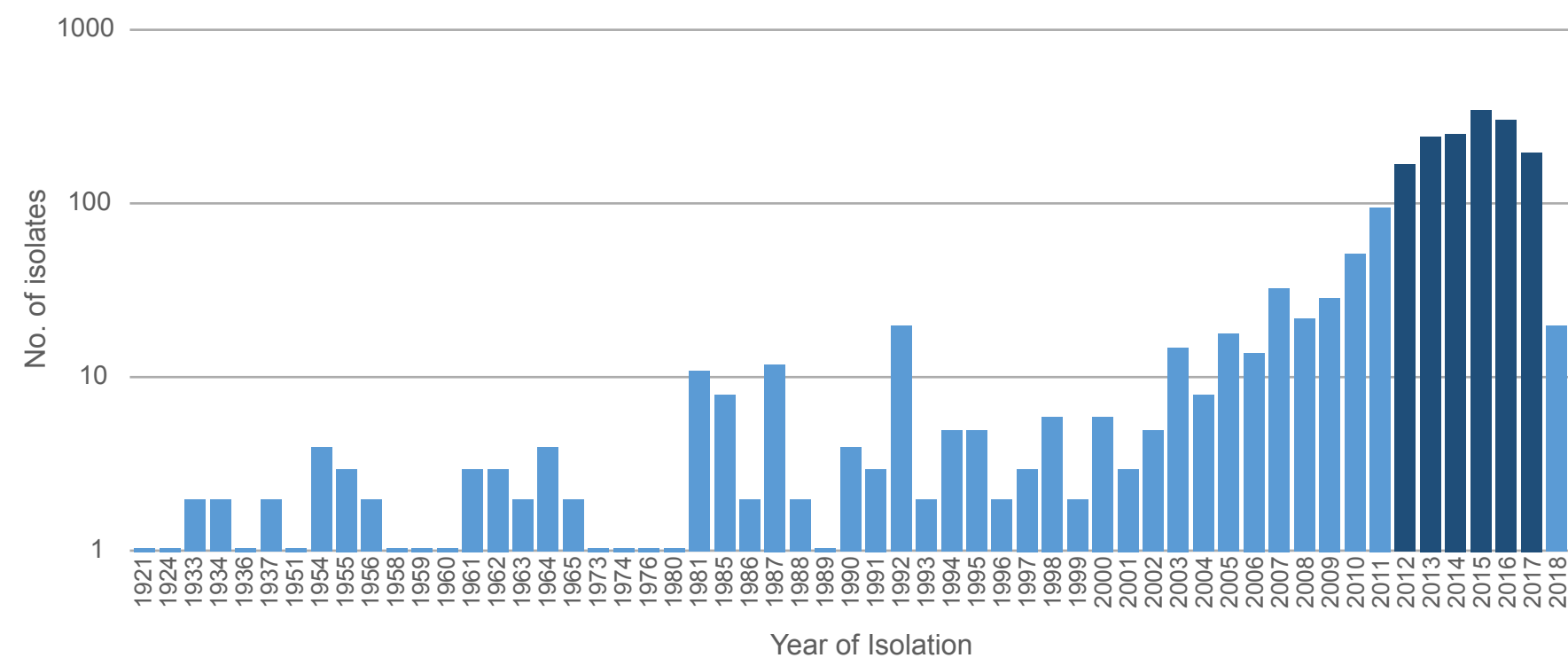
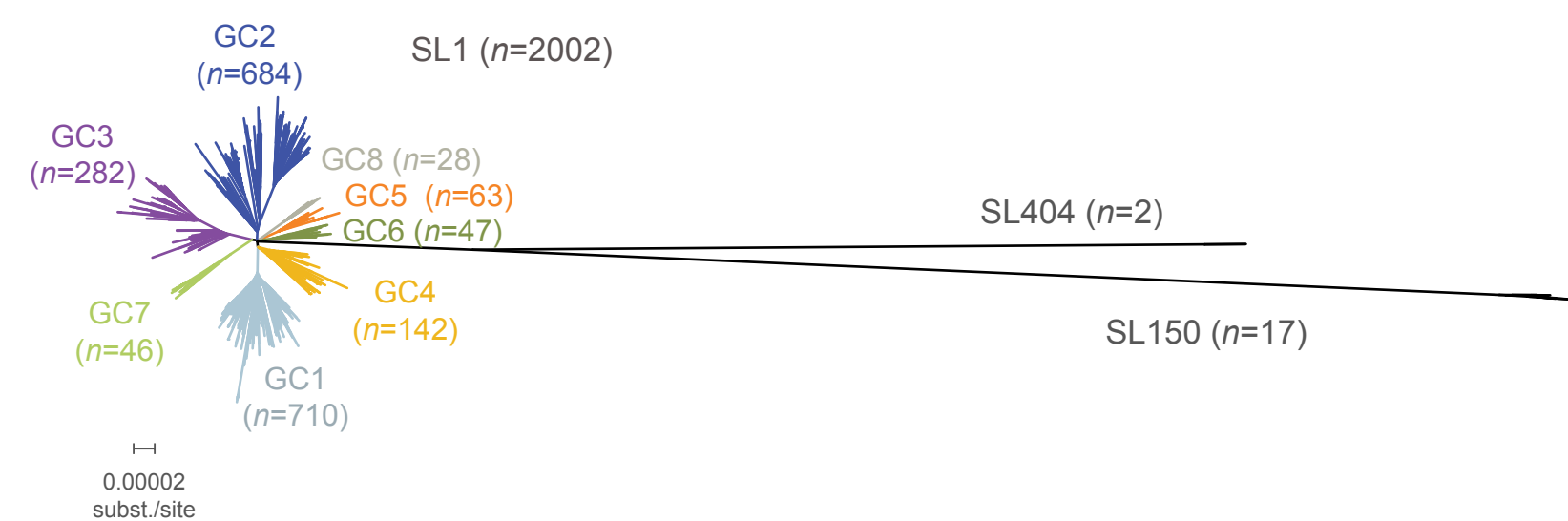
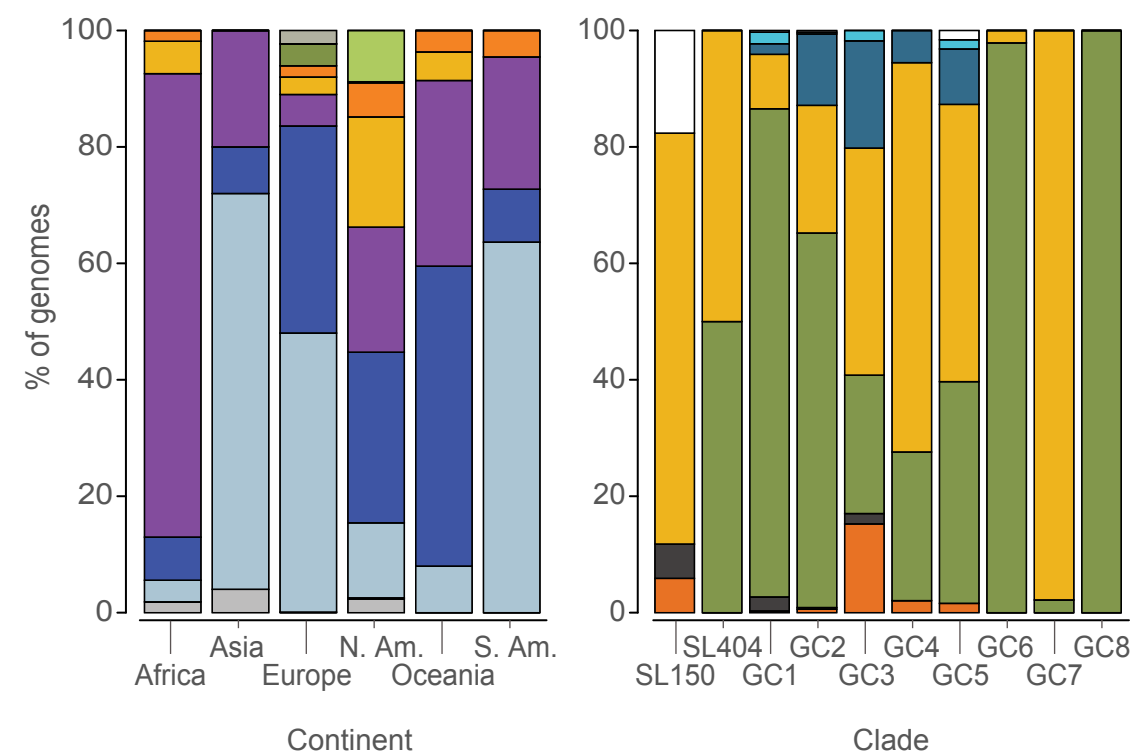
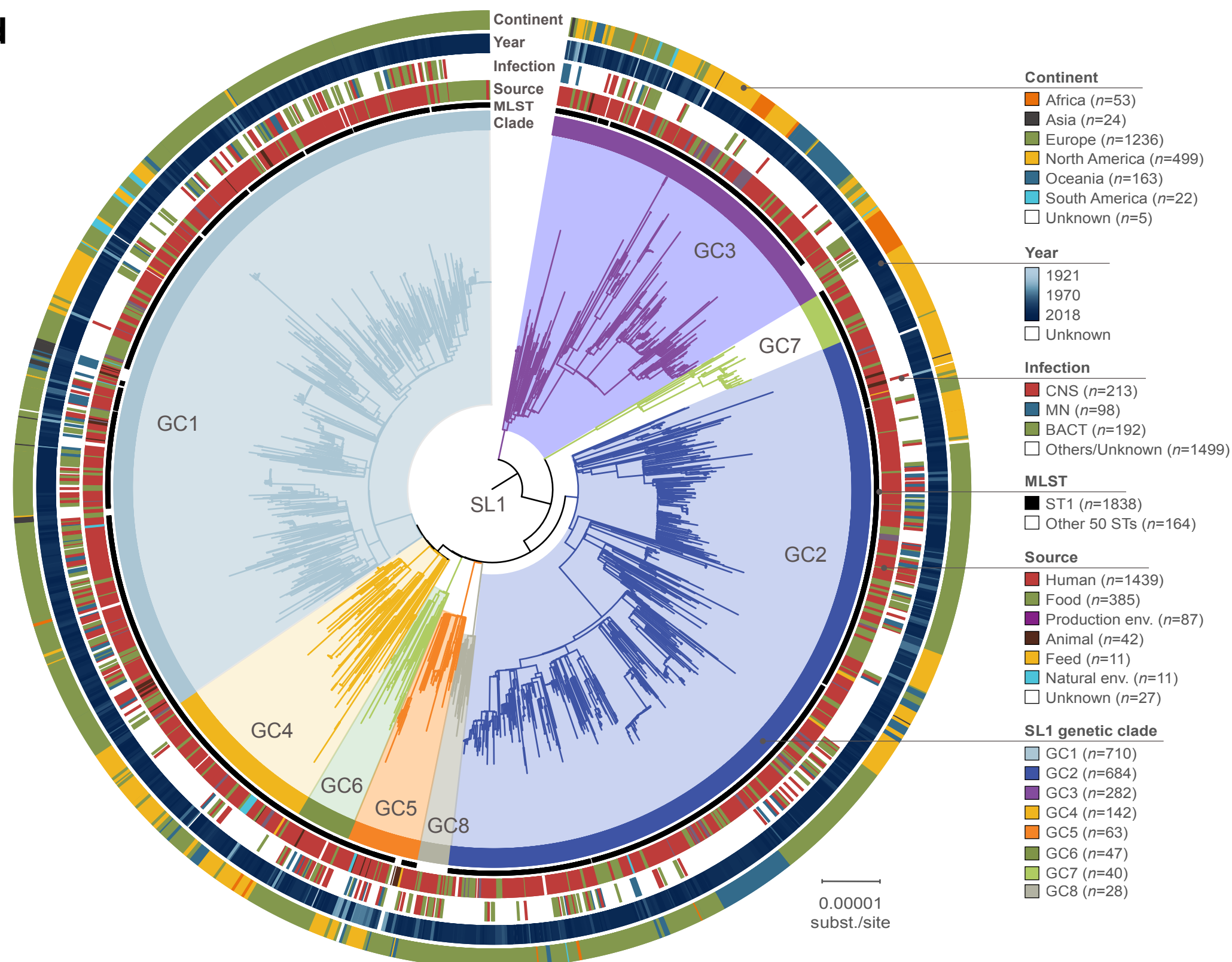
699

700 **Figure 4. Transmission dynamics of sublineage SL1**

701 **a.** Each point summarizes the relative risk that a pair of isolates has a MRCA within a defined
702 timeframe and between different spatial scales: within the same country (within the same
703 continent or within different continents), relative to the risk that a pair of isolates from countries
704 separated by >1000km have a MRCA in the same range (set as the reference value, 'ref'). Error
705 bars represent the 95% confidence intervals, based on 100 bootstrap time-calibrated trees. **b.**
706 Proportion of pairs of isolates within the same country (France) sharing a MRCA of 5 or less
707 years in function of the spatial distance within and between administrative departments (shown in
708 the map). The green line indicates the mean proportion of genetically close strains regardless the
709 geographical location. **c.** Left: relative risk for a pair of isolates to share a MRCA of 5 or less
710 years when both are coming from Paris to when coming from another department (set as reference
711 value) ($p=0.43$). Right: relative risk for a pair of isolates to share a MRCA of 5 or less years
712 when coming from the same department in France, except Paris, compared to when coming from
713 different departments (set as reference value) ($p<0.001$, see Material and Methods for details).

Figure 1**a**

bioRxiv preprint doi: <https://doi.org/10.1101/2020.12.18.423387>; this version posted December 20, 2020. The copyright holder for this preprint (which was not certified by peer review) is the author/funder. All rights reserved. No reuse allowed without permission.

b**c****e****d****Figure 1. Geographical and temporal distribution of the isolates used in this study (N=2,021) and phylogenetic analyses**

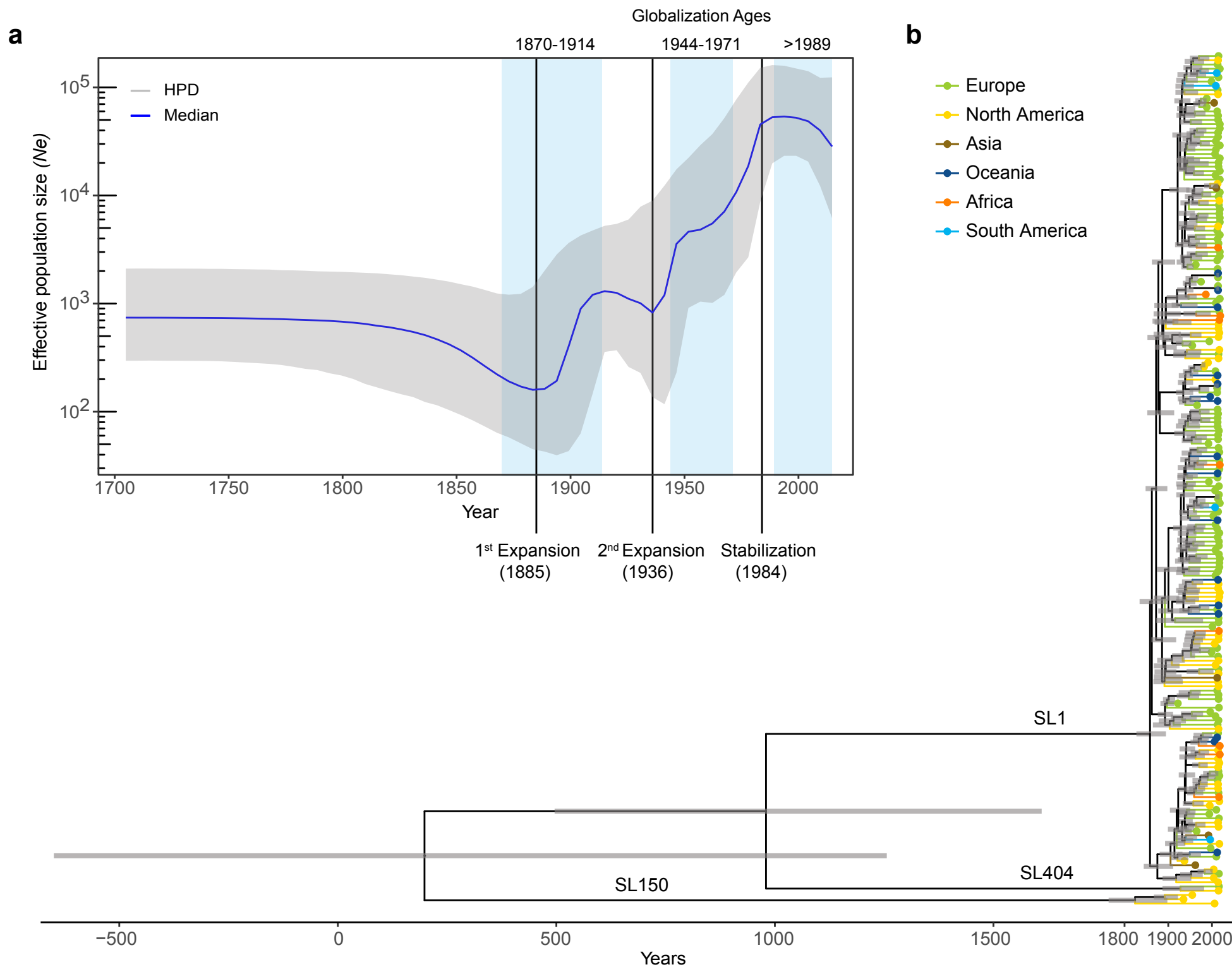
a. Geographical distribution and source distribution. Sampled countries are colored in blue, with hue gradient according to the number of isolates. Pie charts are proportional to the number of isolates sampled in each continent and represent the repartition of sample source types, using the source color key indicated in panel d. Out of 2,021 genomes, 8 isolates had unknown sampling location and are not shown in the map.

b. Temporal distribution of isolates collected in this study. Darker blue bars indicate the period for which exhaustive clinical sampling was obtained for 7 countries spanning 3 continents (2012-2017; US, FR, UK, DK, NL, AU, NZ).

c. Unrooted maximum-likelihood phylogenetic tree of 2,021 *Lm*-CC1 genomes. The tree was generated from analysis (GTR+F+G4 model, 1000 ultra-fast bootstraps) of a 1.29 Mb recombination-purged core genome alignment.

d. Midpoint rooted maximum-likelihood phylogenetic tree of 2,002 SL1 genomes based on a recombination-purged core genome alignment of 1.29 Mb. The four external rings indicate the world region, year, type of infection and source type, respectively. The two inner rings indicate ST1 isolates and the 8 SL1 genetic clades identified in this study, respectively.

e. Percentage of genomes by world region (left) and phylogroup (right). Partitions are colored by world regions and phylogroup, using the same color code as in panel d.

Figure 2**Figure 2. Bayesian temporal and demographic analyses on a representative 200 isolate dataset**

a. Bayesian skyline plot (BSP) with the estimation of *Lm-CC1* effective population size (N_e). The y-axis refers to the predicted number of individuals (log scale) and the x-axis to the timescale (in years). The median population size is marked in blue with its 95% high posterior density (HDP) in gray. Blue vertical panels delimitate the three globalization ages (1870-1914, 1944-1971, 1989-present). **b.** Bayesian time-calibrated tree. Nodes represent the estimated mean divergence times and gray bars represent the 95% HPD confidence intervals of node age. Scale indicates time (in years). Terminal branches and tips are colored by continents, as indicated in the key panel.

Figure 3

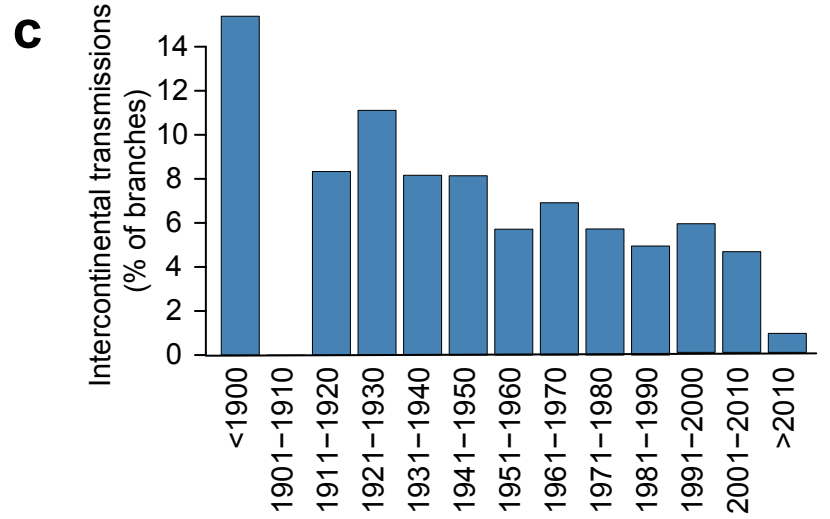
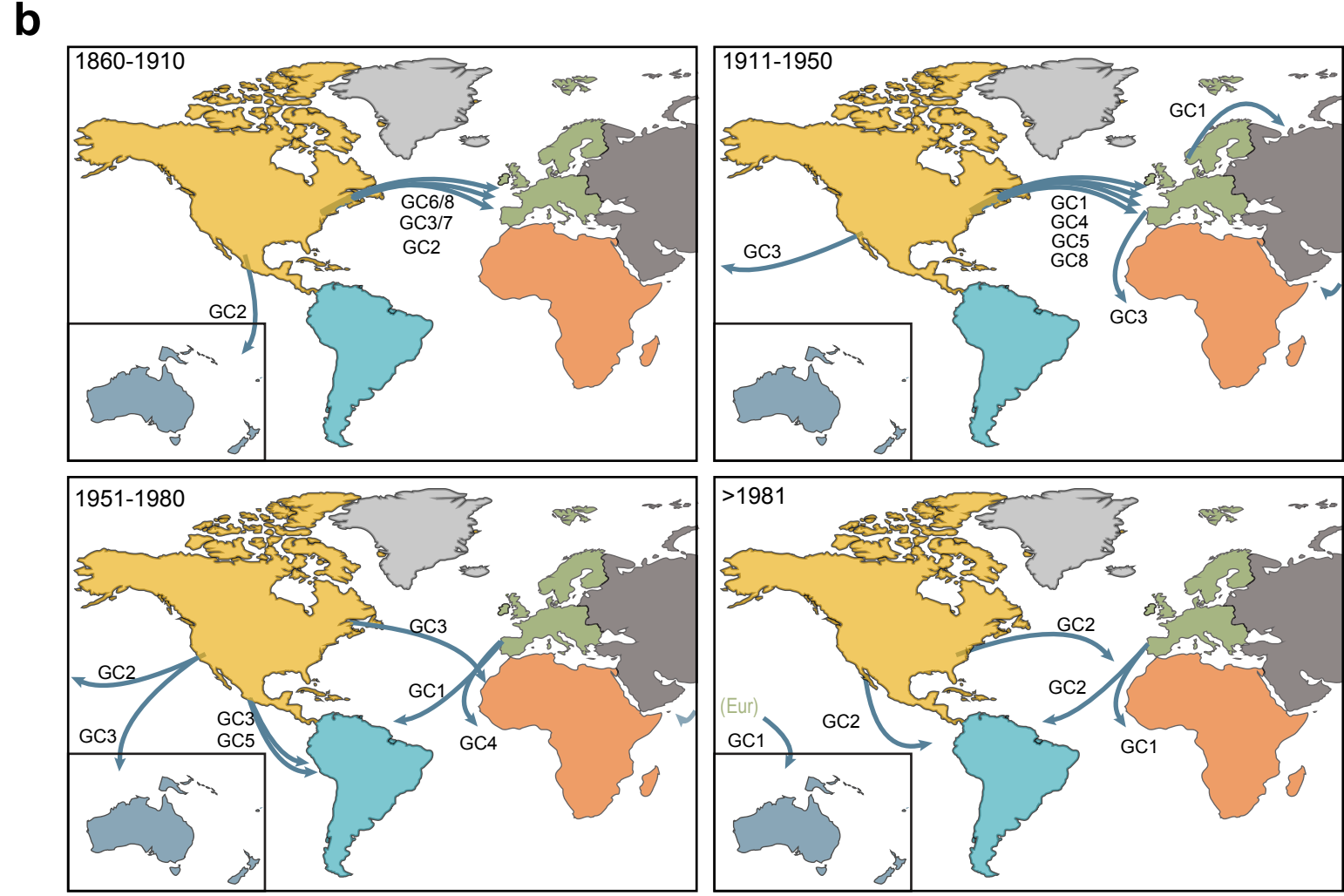
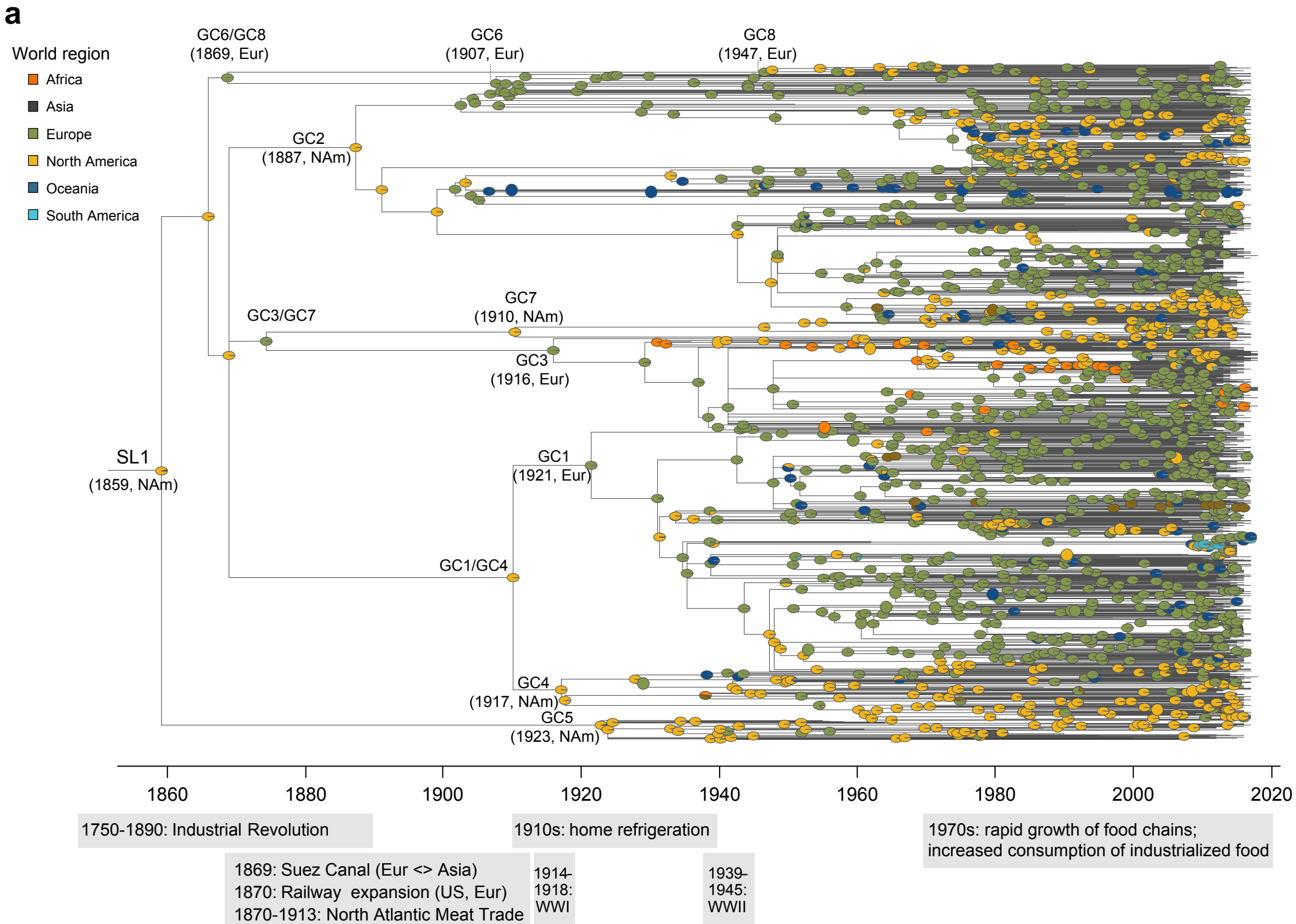
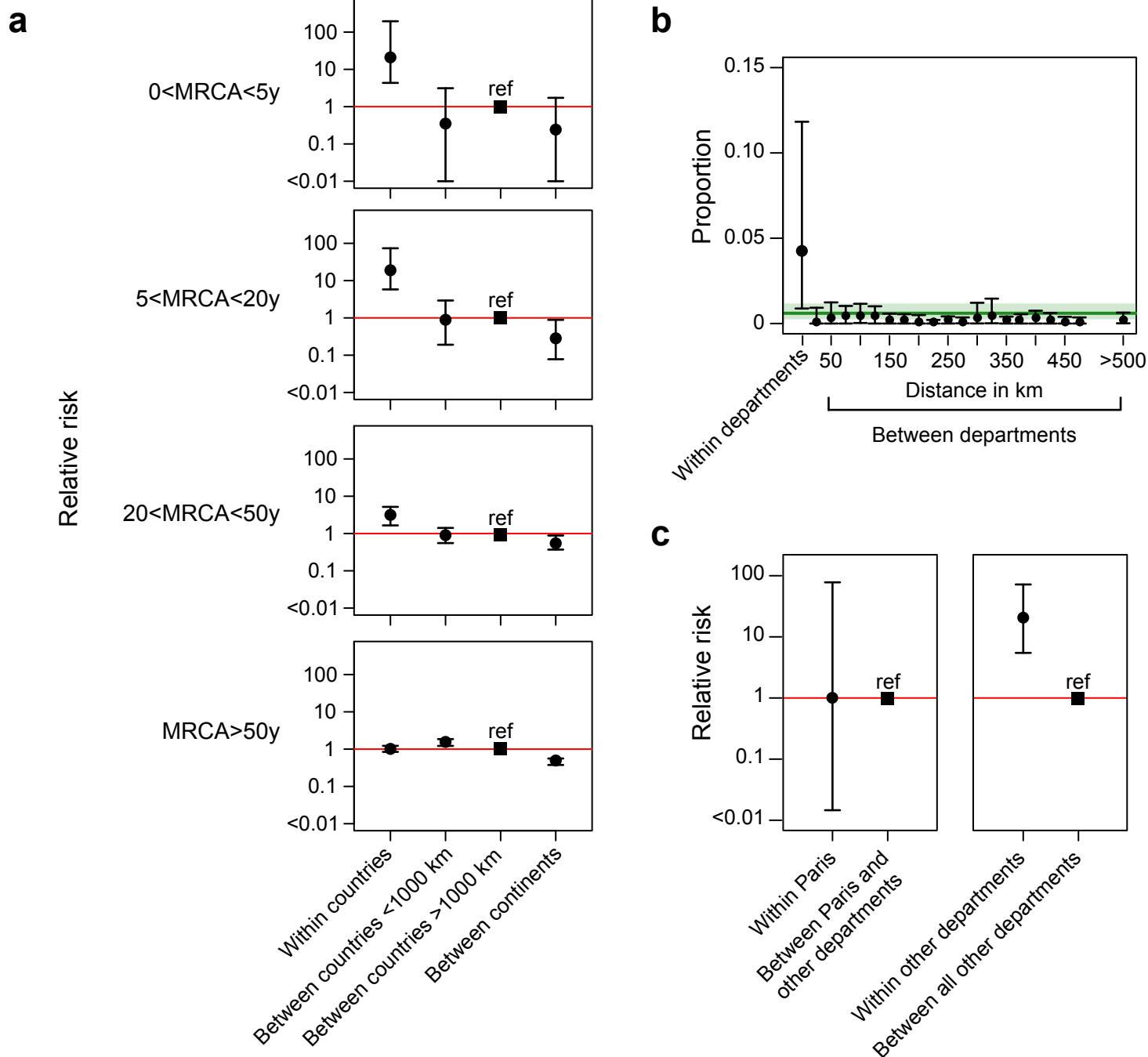


Figure 3. Phylogeography of sublineage SL1
a. Time-calibrated phylogeny based on the 1956 SL1 genomes. Pies at the nodes represent the probability of ancestral geographical locations, estimate using PastML using the MPPA method with an F81-like model. **b.** Inferred spread of SL1 populations across continents. The first introductions of each phylogroup are represented by arrows from their estimated world region origin. **c.** Proportion of inter-continental transitions per 10-year bins, normalized by the total number of phylogenetic branches per bin.

Figure 4**Figure 4. Transmission dynamics of sublineage SL1**

a. Each point summarizes the relative risk that a pair of isolates has a MRCA within a defined timeframe and between different spatial scales (within the same country, within the same continent or within different continents), relative to the risk that a pair of isolates from countries separated by >1000km have a MRCA in the same range (set as the reference value, ‘ref’). Error bars represent the 95% confidence intervals, based on 100 bootstrap time-calibrated trees. **b.** Proportion of pairs of isolates within the same country (France) sharing a MRCA of 5 or less years in function of the spatial distance within and between administrative departments (shown in the map). The green line indicates the mean proportion of genetically close strains regardless the geographical location. **c.** Left: relative risk for a pair of isolates to share a MRCA of 5 or less years when both are coming from Paris to when coming from another department ($p=0.43$). Right: relative risk for a pair of isolates to share a MRCA of 5 or less years when coming from the same department in France, except Paris, compared to when coming from different departments ($p<0.001$, see Material and Methods for details).

1 **Emergence and global spread of the main *Listeria monocytogenes* clinical clonal**
2 **complex**

3

4 Alexandra Moura, Noémie Lefrancq, Alexandre Leclercq, Thierry Wirth, Vítor Borges, Brent
5 Gilpin, Timothy J. Dallman, Joachim Frey, Eelco Franz, Eva M. Nielsen, Juno Thomas, Arthur
6 Pightling, Benjamin P. Howden, Cheryl L. Tarr, Peter Gerner-Smidt, Simon Cauchemez, Henrik
7 Salje, Sylvain Brisse, Marc Lecuit, for the *Listeria* CC1 Study Group

8

9

SUPPLEMENTARY MATERIAL

10 **Table of Contents**

11

12	1. Supplementary tables.....	2
13	Table S1. Isolate included in this study.	2
14	Table S2. Genetic characteristics of CC1 sublineages and SL1 genetic clades.	3
15	Table S3. Sublineage-specific genes present in at least 50% of isolates.	4
16	Table S4. SL1 genetic clades-specific genes present in at least 50% of isolates.	5
17	Table S5. Human-associated significant loci, as determined by treeWAS.	6
18		
19	2. Supplementary figures	7
20	Figure S1. Frequency of most prevalent clonal complexes among different environments.	7
21	Figure S2. Genome metrics of isolates included in this study.	8
22	Figure S3. Core genome multilocus sequence typing (cgMLST) analyses.	9
23	Figure S4. Phylogenetic analysis based on whole genome SNP analyses.	10
24	Figure S5. Genetic diversity among <i>Lm</i> -CC1 isolates	11
25	Figure S6. Distribution of <i>Lm</i> -CC1 isolates per clade, world regions and source types.....	12
26	Figure S7. CC1 pangenome analysis	13
27	Figure S8. Temporal analyses on a representative dataset of 200 isolates.	14
28	Figure S9. Benchmarking of dating methods.....	15
29	Figure S10. Phylogeography inference of <i>Lm</i> -CC1	16
30	Figure S11. Cattle demographics	17
31	Figure S12. French administrative departments (<i>départements</i>)	18
32	Figure S13. SL1 transmission dynamics within country (France).....	19

33

34

35

36 **1. Supplementary tables**

37

38 **Table S1. Isolates included in this study. [[xls](#)]**

39 **Table S2. Genetic characteristics of CC1 sublineages and SL1 genetic clades and statistics by world region.**

40

	<i>n</i>	cgMLST allelic distances	cg1748 SNP distances (1.29 Mb, 11,976 ATGC sites)				wgF2365 SNP distances (2.28 M, 29,108 ATGC sites)			
		mean ± stdev	mean ± stdev	Tajima's D	nucleotide diversity	haplotype diversity	mean ± stdev	Tajima's D	nucleotide diversity	haplotype diversity
Phylogroup SL1	2002	68 ± 23.27	38 ± 14.8	-2.69	4.33	0.966	80 ± 27.4	-2.77	63.31	0.999
SL404	2	57	50	nd	50.00	1.000	107	nd	107.00	1.000
SL150	17	42 ± 16.90	38 ± 16.8	-1.46	33.41	1.000	86 ± 30.9	-1.70	79.62	1.000
GC1	710	39 ± 11.16	32 ± 9.5	-2.78	10.13	0.992	67 ± 15.9	-2.82	49.05	0.997
GC2	684	51 ± 18.03	45 ± 16.4	-2.70	14.92	0.991	92 ± 30.6	-2.80	48.27	0.997
GC3	282	47 ± 17.41	38 ± 14.8	-2.63	12.79	0.991	85 ± 25.8	-2.77	65.25	0.999
GC4	142	46 ± 19.97	39 ± 17.3	-2.59	24.68	0.990	100 ± 29.9	-2.73	86.73	0.992
GC5	63	34 ± 13.23	28 ± 11.3	-2.38	22.38	0.995	73 ± 23.5	-2.51	68.35	0.999
GC6	47	45 ± 16.00	36 ± 13.6	-2.22	32.66	0.988	79 ± 25.6	-2.29	73.67	0.990
GC7	46	28 ± 24.28	24 ± 20.8	-1.60	19.97	0.966	63 ± 51.7	-2.03	58.94	0.998
GC8	28	29 ± 7.94	25 ± 6.7	-2.39	23.18	0.997	50 ± 10.5	-2.47	45.31	1.000
World Region Africa	54	66 ± 91.55	64 ± 148.7	-2.72	41.06	0.962	146 ± 220.0	-2.62	119.17	0.997
Asia	25	85 ± 119.86	100 ± 204.3	-2.55	67.85	0.990	187 ± 332.3	-2.49	180.76	1.000
Europe	1236	61 ± 24.50	53 ± 28.9	-2.74	13.42	0.995	110 ± 44.9	-2.78	59.04	0.999
North America	513	92 ± 92.77	96 ± 160.3	-2.58	28.06	0.992	194 ± 232.0	-2.68	164.93	0.998
South America	22	63 ± 31.91	52 ± 27.6	-1.39	47.01	0.987	117 ± 55.0	-1.57	114.57	0.996
Oceania	22	63 ± 31.91	52 ± 27.6	-1.39	47.01	0.987	117 ± 55.0	-1.57	114.57	0.996

41

42 **Table S3. Sublineage-specific genes present in at least 50% of isolates.** Gray shades

43 highlight genes within the same genomic context.

Remarks	Roary_family	Reference locus	Ortholog	Annotation	Length (nt)	No. isolates	% Isolates (in SL)	#Order in contig
exclusively in SL1	group_2369	ID32421_02477	lmo0671	hypothetical protein	293	1852	93%	
exclusively in SL404	group_7853	ID31663_01719	lmo0804	hypothetical protein	176	2	100%	1067
	group_7852	ID31663_01117	LMOF2365_0494	hypothetical protein	2150	1	50%	6972
exclusively in SL150	group_897	ID32037_02878		hypothetical protein	260	16	94%	1226
	group_6423	ID32037_02875	LMOSA_10	hypothetical protein	467	16	94%	1229
	group_5149	ID32037_02874	LMOSA_20	replication-associated protein	305	14	82%	1230
	group_6471	ID32037_02873	LMOF2365_0352	hypothetical protein	284	12	71%	1231
	group_6421	ID32037_02872		hypothetical protein	314	16	94%	1232
	group_5148	ID32037_02871		hypothetical protein	116	12	71%	1233
	group_6420	ID32037_02870	lmo0339	inorganic pyrophosphatase	371	16	94%	1234
	group_6409	ID32037_00117		hypothetical protein	290	14	82%	3282
	group_2611	ID32037_00115	lmo2044	peptide ABC transporter substrate-binding protein	1664	13	76%	3284
	group_6408	ID32037_00121	lmo2749	glutamine amidotransferase	572	16	94%	3302
	group_6406	ID32037_00123	lmo2375	hypothetical protein	395	16	94%	3304
	group_6417	ID32037_01337		hypothetical protein	110	16	94%	4171
	group_6418	ID32037_01335	lmo2688	cell division protein FtsW	1130	16	94%	4175
exclusively in SL150 & SL404	recD	ID32037_02916	LMOSA_12110	DNA helicase; RecBCD enzyme subunit RecD	1355-3608	18	95%	2391
(absent in SL1)	group_5134	ID32037_02915		hypothetical protein	1061-1340	18	95%	2392
	group_6411	ID32037_02914	lmo0303	putative secreted, lysin rich protein	551	18	95%	2393
	group_6412	ID32037_02912	lmo0305	L-allo-threonine aldolase	1082	18	95%	2395
	group_6413	ID32037_02911	lmo0306	hypothetical protein	467	18	95%	2396
	group_6415	ID32037_02907	lmo0310	hypothetical protein	1076	17	89%	2400
exclusively in SL1 & SL404	group_152	ID32421_02841	LMOF2365_0349	cell wall surface anchor family protein (LPxTG motif)	293-3221	1380	69%	2433
(absent in SL150)	group_1481	ID32421_01841	LMOF2365_2341	aminotransferase, class I	221-1166	1936	97%	3295
	group_4436	ID32421_01836	lmo2375	hypothetical protein	263-392	2004	100%	3309
	group_378	ID32421_01835		reverse transcriptase	302-1385	1977	99%	3310
	group_1844	ID32421_00303	lmo2688	cell division protein FtsW	758-1130	1009	50%	4177
	group_1501	ID32421_00308	LMOF2365_2670	N-acetylmuramoyl-L-alanine amidase, family 4	1100-1775	1450	72%	4183
exclusively in SL1 & SL150	group_1153	ID32421_02877	lmo0297	transcriptional antiterminator BglG	593-1871	1991	99%	2373
(absent in SL404)	sau3AIR	ID32421_02872		Type-2 restriction enzyme Sau3AI	152-1667	1990	99%	2379
	group_4596	ID32421_02871	LMOF2365_0326	transcriptional regulator	164-206	2000	99%	2382
	group_1899	ID32421_02870	LMOF2365_0327	cytosine-specific methyltransferase	131-1409	1988	98%	2384
	group_1900	ID32421_02869	LMOF2365_0328	hypothetical protein	236-854	1952	97%	2386
	group_1572	ID32421_02868	LMOF2365_0329	putative lipoprotein	197-554	1993	99%	2387
	group_1901	ID32421_02867	LMOF2365_0330	threonine aldolase	305-1079	2000	99%	2388
	group_3681	ID32421_02866	LMOF2365_0331	peptidase, M48 family	464-920	2001	99%	2389
	group_1342	ID32421_02360	lmo0804	hypothetical protein	155-959	1997	99%	3058
	group_5703	ID32037_01341		hypothetical protein	89	1021	51%	4167
	group_2203	ID32421_00342		hypothetical protein	329-632	1999	99%	4215
	group_596	ID32421_00343		hypothetical protein	248-1286	1837	91%	4216
	group_791	ID32421_00344		hypothetical protein	455-983	1787	89%	4218
	group_5708	ID32421_00345		hypothetical protein	299	1991	99%	4222
	group_5709	ID32421_00346		hypothetical protein	359-359	1995	99%	4223
	group_2733	ID32421_00347		hypothetical protein	407-773	1999	99%	4224
	group_3456	ID32421_00351	lmo2724	3-demethylubiquinone-9 3-methyltransferase	323-443	1986	98%	4229
	group_2255	ID32421_02154	LMOF2365_0239	dihydrouridine synthase family protein	209-995	1585	79%	4765
	group_81	ID32421_00680	LMOF2365_0495	putative lipoprotein	155-2159	1244	62%	7056
	group_2830	ID32421_00615	lmo2084	aminoglycoside phosphotransferase	455-476	1862	92%	6967
	group_3057	ID32421_01316	lmo1343	competence protein ComGE	284-284	2004	99%	8031
	group_1982	ID32421_01310	LMOF2365_1365	glycine cleavage system T protein GcvT	797-1088	2009	100%	8039
	group_555	ID32421_02213	lmo1721	transcriptional regulator	788-2771	1943	96%	8392
	group_2258	ID32037_00061	LMOF2365_1741	transcriptional regulator, TetR family	188-584	1950	97%	8398
	group_1540	ID32421_02218	lmo1715	methyltransferase	185-668	1940	96%	8399
	group_1048	ID32421_00984	lmo0738	PTS beta-glucoside transporter subunit IIABC	698-1448	1879	93%	8654
	group_5905	ID32421_00985	lmo0116	hypothetical protein_lmaC_phageA118	167	2015	100%	8657
	group_1669	ID32421_00989	lmo1655	vanZ-like protein	128-563	1889	94%	9030

44
45

Table S4. SL1 genetic clades-specific genes present in at least 50% of isolates.

Clades-specific genes were only found in GC3 and GC7. Gray shadows highlight genes within the same genomic context.

Remarks	Roary_family	Reference locus	Ortholog	Annotation	Length (nt)	No. isolates	% Isolates (in GC)	#Order in contig
exclusively in GC3	group_1376	ID106_01313		fibrinogen-binding protein	1562-2693	215	76%	7335
	group_5934	ID106_01309		hypothetical protein	1301	271	96%	7345
	group_5933	ID106_01308		hypothetical protein	485	271	96%	7346
	group_4885	ID106_01307		hypothetical protein	212-374	271	96%	7347
	group_5932	ID106_01306		hypothetical protein	1019	271	96%	7348
	group_5931	ID106_01305		hypothetical protein	338	271	96%	7349
	group_4884	ID106_01304		hypothetical protein	269-686	271	96%	7350
	group_3147	ID106_01302		hypothetical protein	1253-1769	269	95%	7356
	group_3146	ID106_01301		P60 protein	812-1025	271	96%	7358
	group_2504	ID106_01300		cadmium resistance protein_cadA	1403-2105	268	95%	7359
	group_4029	ID106_01299		cadmium efflux system accessory protein_cadC	236-356	267	95%	7360
	group_5930	ID106_01298		ABC transporter- permease protein	770	270	96%	7361
	group_4883	ID106_01297		ABC transporter- ATP-binding protein	278-935	271	96%	7362
	group_5929	ID106_01296		hypothetical protein	173	269	95%	7363
	group_5928	ID106_01295		dihydroliipoamide dehydrogenase	1673	271	96%	7364
	acr3_2	ID106_01293		Arsenical-resistance protein Acr3	1076	271	96%	7370
	group_5926	ID106_01291		ArsR family transcriptional regulator	365	271	96%	7379
	arsD_1	ID106_01290		Arsenical resistance operon trans-acting repressor ArsD	371	271	96%	7380
	group_5924	ID106_01289		cadmium efflux system accessory protein_cadC	293	271	96%	7381
	arsA_2	ID106_01288		Arsenical pump-driving ATPase	263-1739	271	96%	7382
arsD_2	ID106_01287		Arsenical resistance operon trans-acting repressor ArsD	311	270	96%	7383	
group_5922	ID106_01286		cystathionine beta-lyase	1142-1142	270	96%	7384	
group_5921	ID106_01285		hypothetical protein	458	254	90%	7385	
group_4882	ID106_01284		hypothetical protein	302-404	256	91%	7386	
exclusively in GC7	group_8396	ID32182_02420		hypothetical protein	326	42	91%	1150

Table S5. Human-associated significant loci, as determined using treeWAS, with a significance threshold of $p < 10^{-5}$.

Gene	Annotation	treeWAS score	Association type	G1P1	G0P0	G1P0	G0P1
group_1361	hypothetical protein	24	positive	1303	88	480	150
group_2465	valyl-tRNA synthetase_valS	22	positive	1300	89	479	153
group_1038	N-acetylmuramoyl-L-alanine amidase	26	positive	1265	96	472	188
group_619	hypothetical protein	23	positive	1175	138	430	278
group_10387	tRNA-Glu(ttc)	25	positive	1041	181	387	412
group_497	hypothetical protein	24	positive	1029	190	378	424
group_1926	transcriptional regulator	25	positive	1024	193	375	429
group_706	hypothetical protein	25	positive	1020	191	377	433
group_1527	hypothetical protein	24	positive	1007	186	382	446
group_209	hypothetical protein	24	positive	866	254	314	587
group_6398	tRNA-Val(tac)	-25	negative	611	246	322	842
group_10476	5S ribosomal RNA	-31	negative	520	253	315	933
group_10390	tRNA-Glu(ttc)	-33	negative	532	276	292	921
group_10432	tRNA-Lys(ttt)	-35	negative	499	289	279	954
group_10162	tRNA-Asn(gtt)	-29	negative	461	309	259	992
group_10094	hypothetical protein	-28	negative	492	362	206	961
group_10662	hypothetical protein	-30	negative	479	358	210	974
group_1927	transcriptional regulator	-25	negative	430	375	193	1023
group_499	hypothetical protein	-23	negative	404	397	171	1049
group_10488	5S ribosomal RNA	-41	negative	282	399	169	1171
group_4211	5S ribosomal RNA (partial)	-37	negative	227	398	170	1226
group_60	putative lipoprotein	-27	negative	188	476	92	1265
group_533	hypothetical protein	-22	negative	74	508	60	1379
group_6404	hypothetical protein	-22	negative	36	518	50	1417

G, genome; P, phenotype; 0 absent, 1 present.

2. Supplementary figures

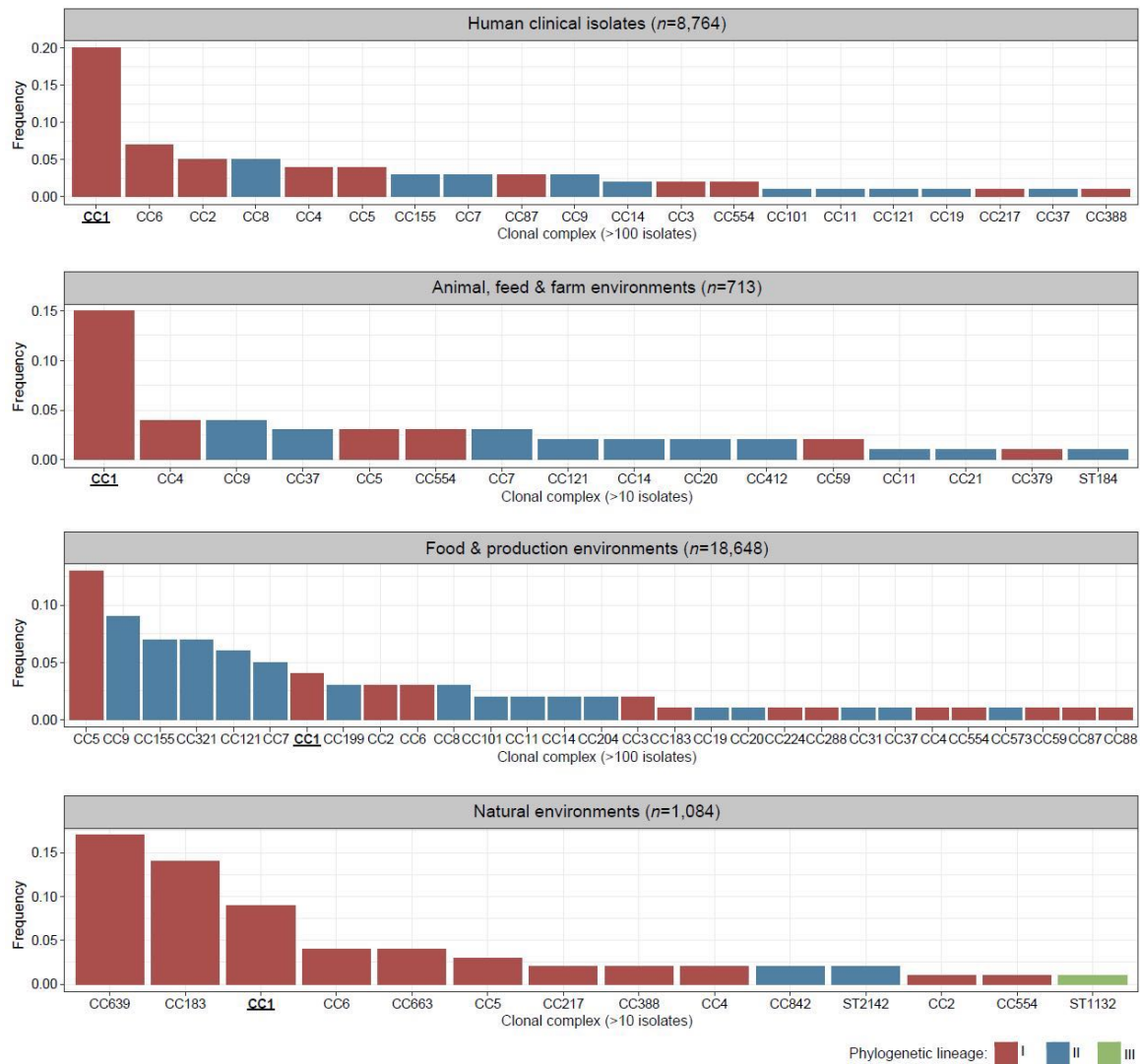


Figure S1. Frequency of most prevalent clonal complexes among different environments. Data collected based on 29,349 *L. monocytogenes* genomes with associated source metadata available on NCBI Sequence Read Archive (as of October 23rd, 2020). MLST typing was performed from reads using the srst2 v.0.1.5 software (<http://katholt.github.io/srst2>) and the BIGSdb-*Lm* profiles database (<https://bigsdb.pasteur.fr/listeria>).

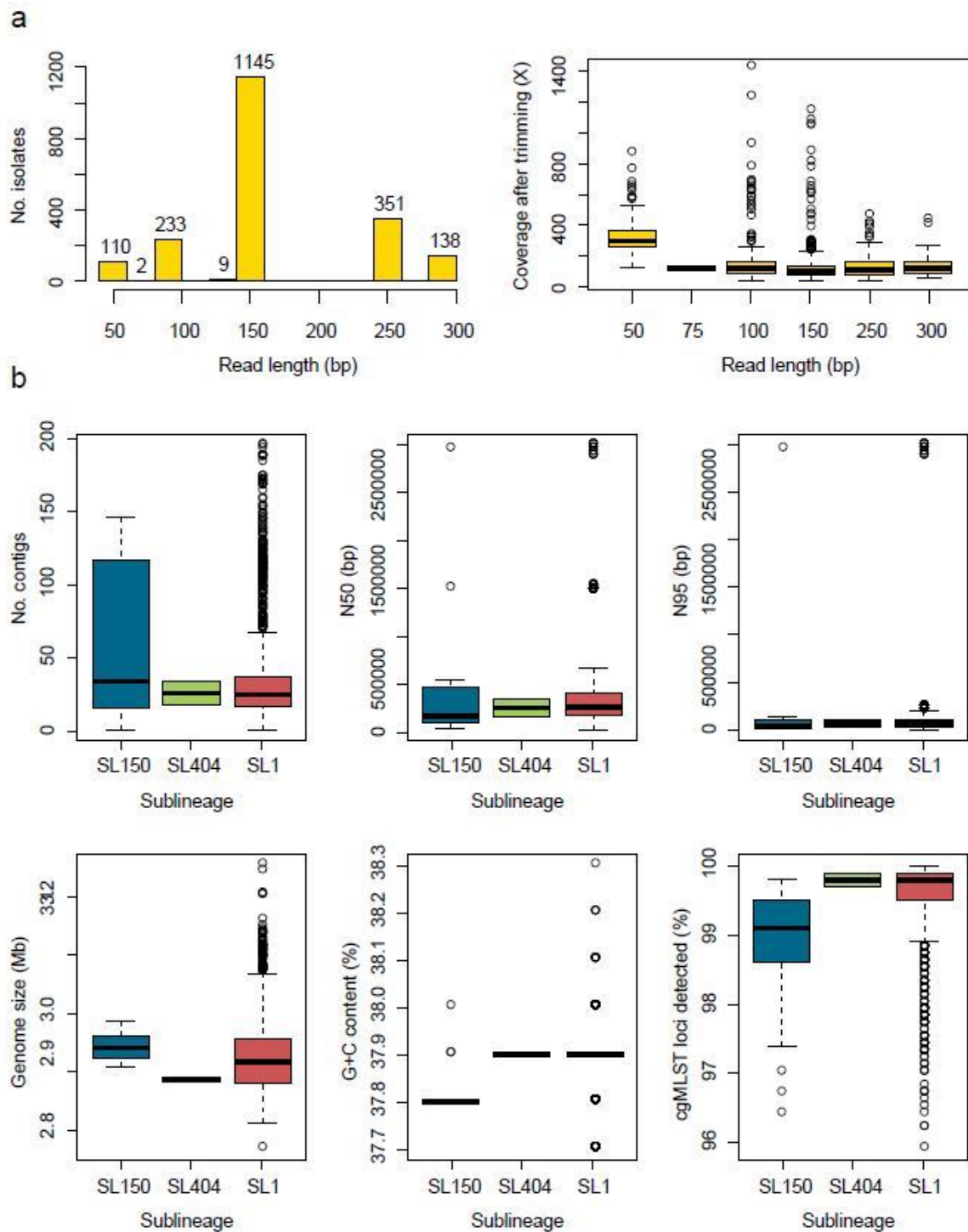


Figure S2. Genome metrics of isolates included in this study.

a) Distribution of isolates per sequence read length (left) and distribution of sequencing coverages after reads quality trimming (right).

b) Assembly metrics per CC1 sublineages, based on the number of contigs, N50 and N95 contig lengths, genome size, G+C content and cgMLST loci detected.

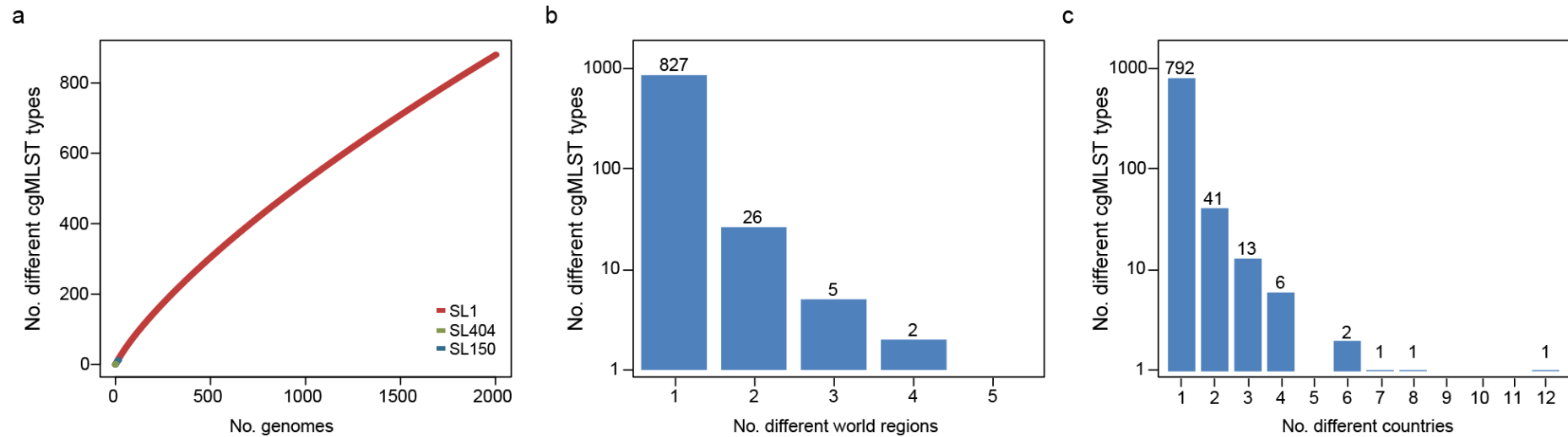


Figure S3. Core genome multilocus sequence typing (cgMLST) analyses.

a) Rarefaction analysis of cgMLST types sampled per sublineage.

b) Number of SL1 cgMLST types per number of different world regions in which they were observed ($n=860$ types with world region information).

c) Number of SL1 cgMLST types per number of different countries in which they were observed ($n=857$ types with country information).

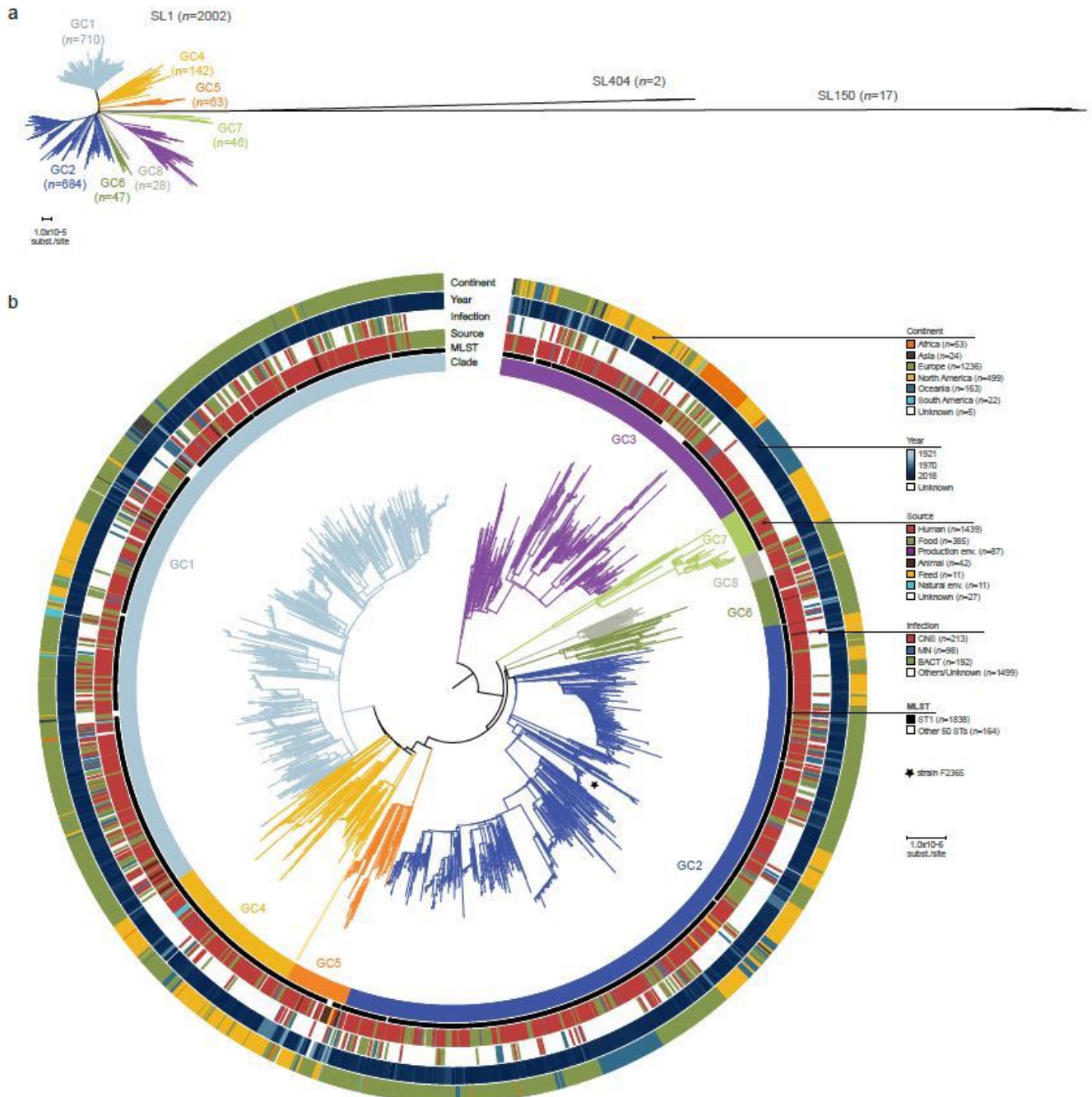


Figure S4. Phylogenetic analysis based on whole genome SNP analyses.

a) Unrooted maximum-likelihood phylogeny (GTR+F+G4 model, 1000 ultra-fast bootstraps, using IQ-Tree^{23,26}) of 2,021 CC1 genomes based on the recombination-purged whole genome SNP alignment of 2.28 Mb.

b) Midpoint rooted maximum-likelihood phylogenetic tree of 2,002 SL1 genomes based on based on the recombination-purged whole genome SNP alignment of 2.28 Mb. The four external rings indicate the world region, year, type of infection and source type, respectively. The two inner rings indicate ST1 isolates and the 8 SL1 genetic clades identified in this study, respectively. The black star highlights the phylogenetic placement of isolate F2365 (accession no. NC_002973.6), used as reference in whole genome read mapping.

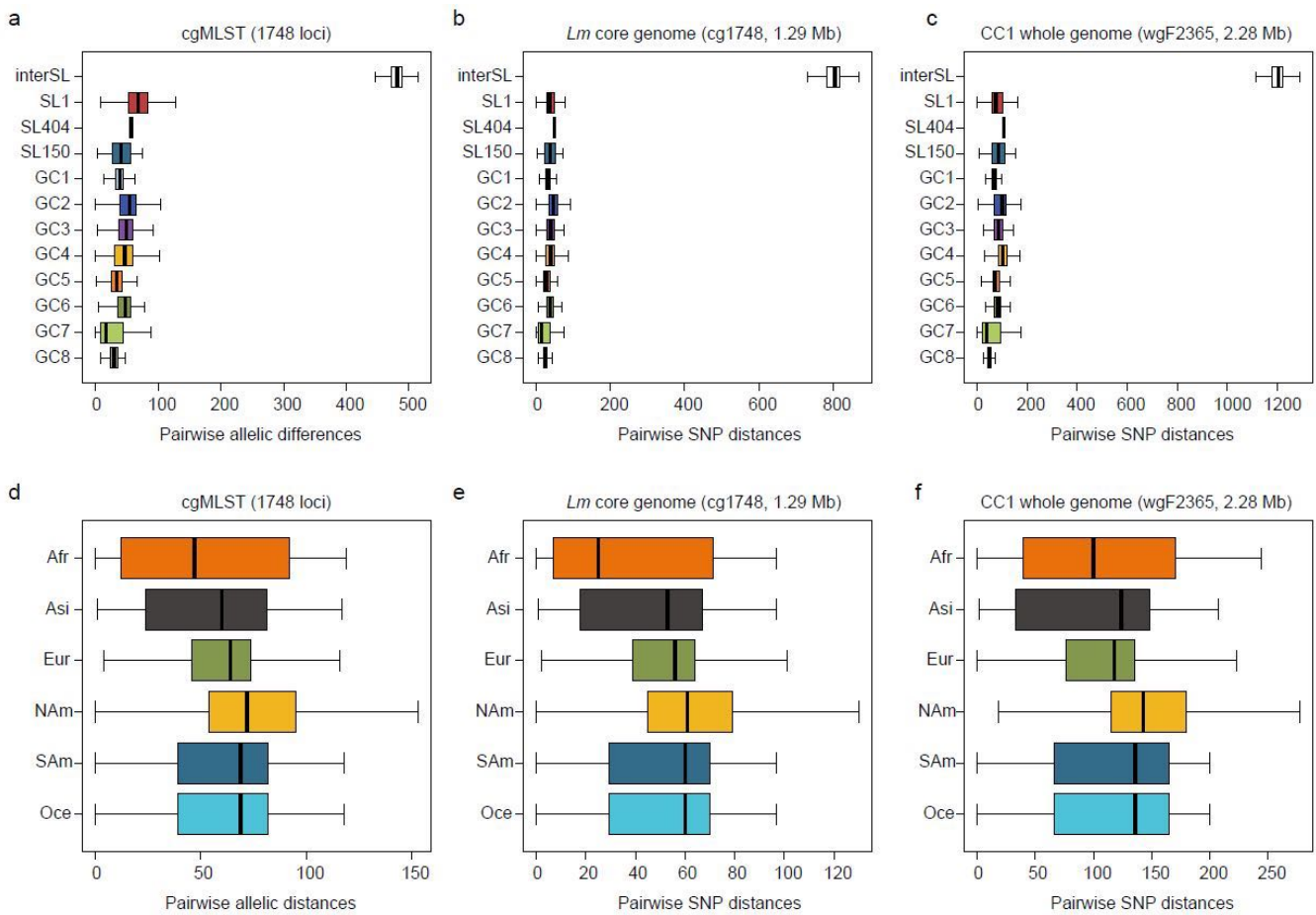


Figure S5. Genetic diversity among *Lm*-CC1 isolates.

Pairwise isolate distances within CC1 phylogroups (top) and world regions (bottom): a,d) pairwise cgMLST allelic distances; b,e) pairwise SNP distances in recombination-purged *Lm* core genome alignment and c,f) recombination-purged CC1 whole genome alignment. Uncalled alleles, Ns and gap alignment positions were ignored in pairwise comparisons. Each box denotes the 25% and 75% quartiles and lines represent the medians. Inter-SL, inter CC1 sublineages; GC#, within SL1 genetic clades; Afr, Africa; Asi, Asia; Eur, Europe; NAm, North America; Sam, South America; Oce, Oceania.

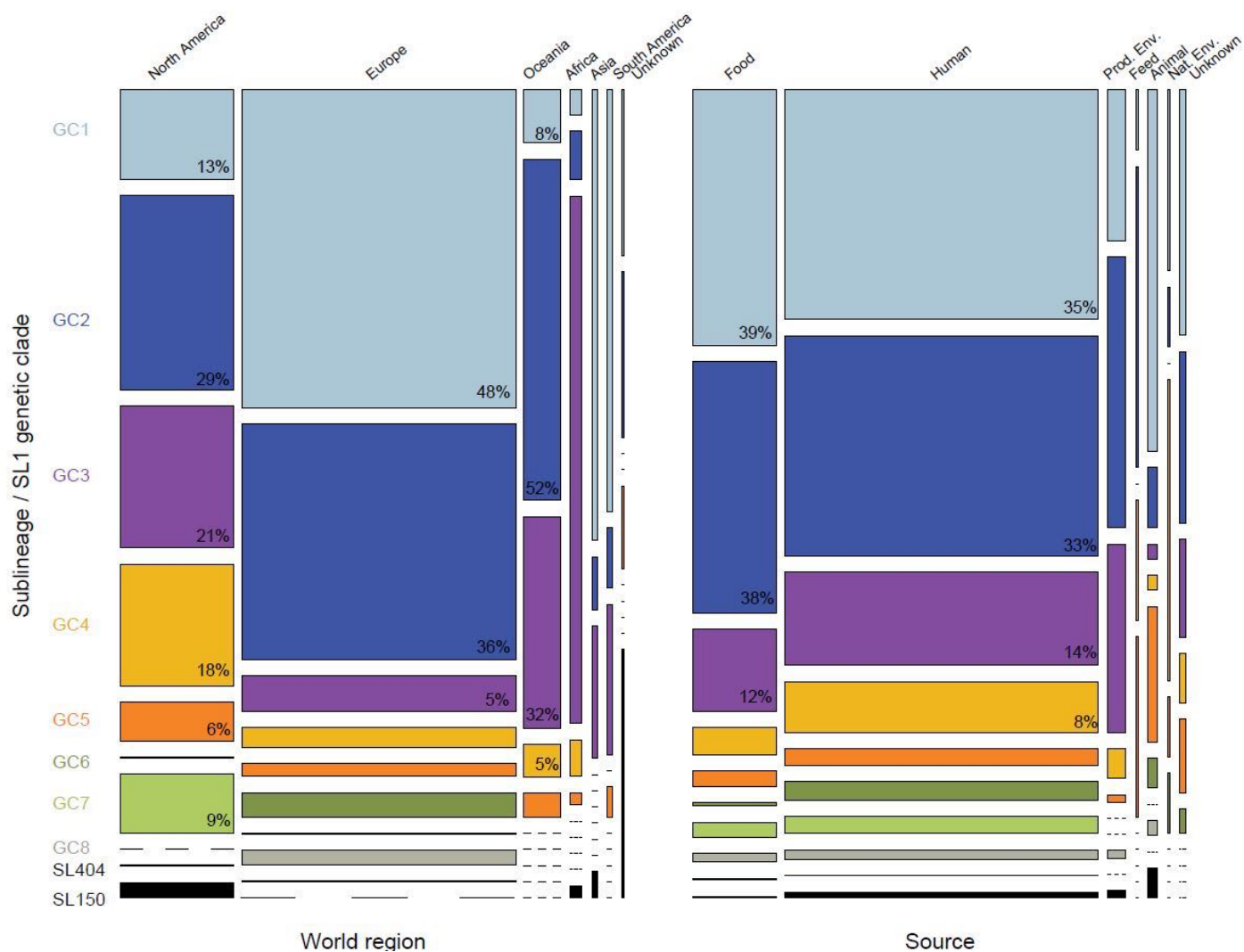


Figure S6. Distribution of *Lm*-CC1 isolates per clade, world regions and source types (N=2,021).

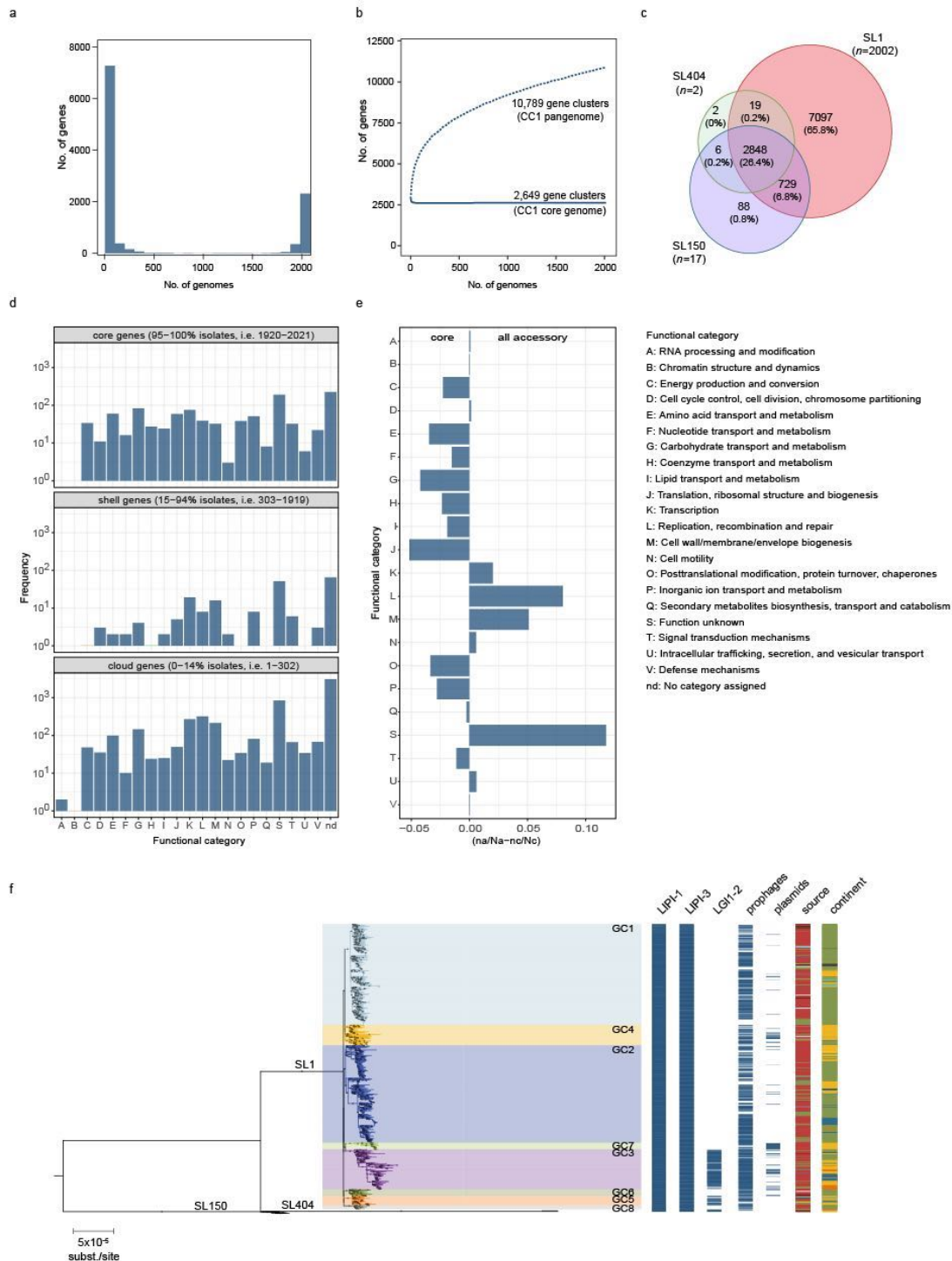


Figure S7. CC1 pangenome analysis.

a) Frequency of sampled gene families. b) Pan- and core gene families sampled. c) Venn diagram showing the number of gene families present in at least 1 sublineage member. d) Distribution of the functional categories of the clusters of orthologous genes across the CC1 pangenome. e) Differential proportion of each assigned COG category in core vs accessory genome, calculated as the difference between the ratio of each category (n) and the total number of hits (N) among each gene pool set, as in $(n_{\text{accessory}}/N_{\text{accessory}} - n_{\text{core}}/N_{\text{core}})$. f) Distribution of *Listeria* genomic islands, prophages and plasmids and across CC1 phylogeny. The midpoint rooted maximum-likelihood phylogenetic tree (GTR+F+G4 model, 1000 ultra-fast bootstraps) was inferred from the 1.29 Mb recombination-purged core genome alignment of 2,021 CC1 genomes. Sources, continents and SL1 clades are colored according to the color codes shown in Figure S4.

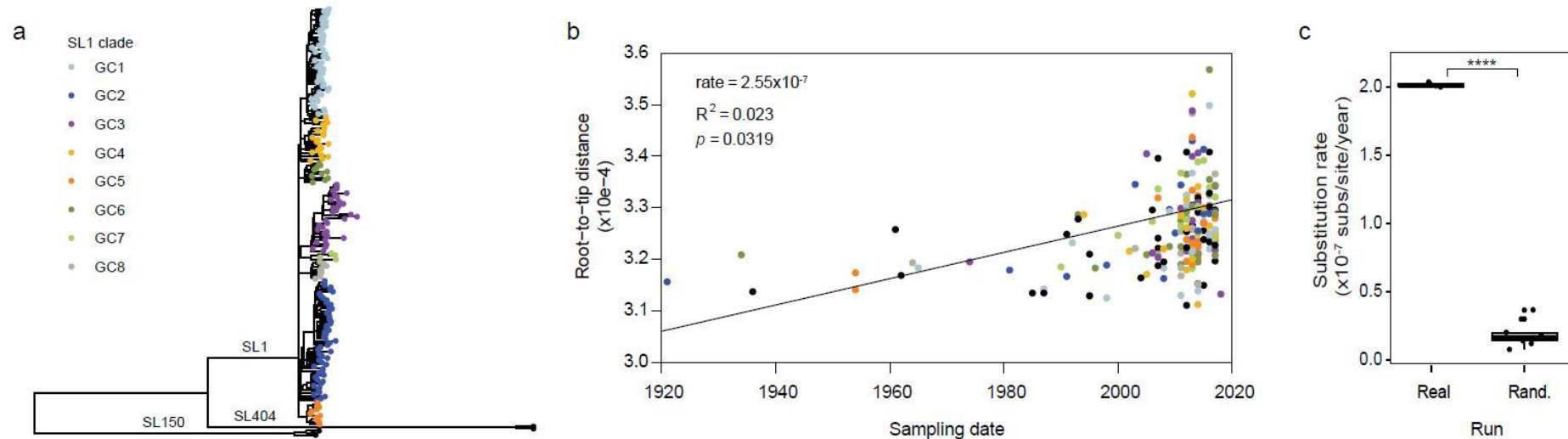


Figure S8. Temporal analyses on a representative dataset of 200 isolates.

a) Maximum likelihood (GTR+F+G4) phylogeny of the representative 200 isolates selected randomly across the CC1 phylogeny. Tips are colored by sublineage and SL1 genetic clades as indicated in the legend. b) Regression analyses showing the root-to-tip genetic distance against sampling date (year). Statistical significance was assessed using the F-test. c) Bayesian molecular clock estimations in real and randomized tip dates (controls). Estimations based on real data were run in triplicates, whereas estimations based on randomized tip datasets were run in 10 replicates. Stars denote statistical significance of $p < 0.0001$, assessed using t-test.

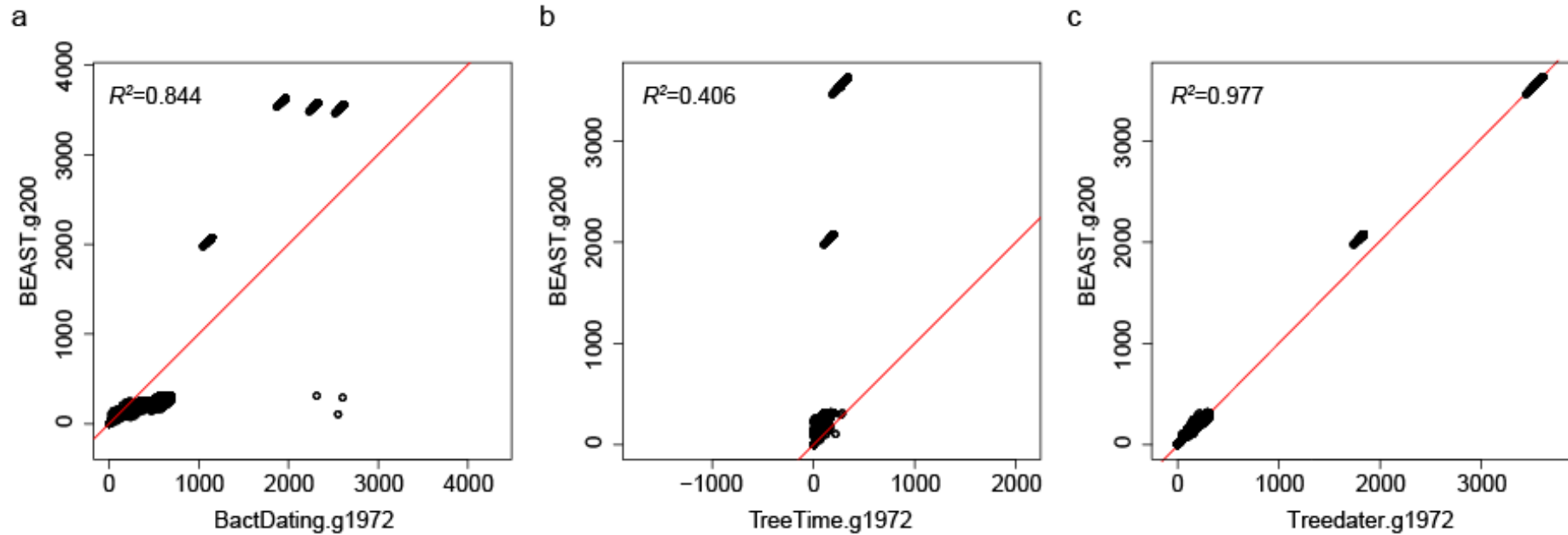


Figure S9. Benchmarking of dating methods.

Cophenetic distances between isolates dated with BEAST and alternative large-scale methods: a) BactDating v.1.0.1, b) Treetime v.0.5.2 and c) Treedater v.0.3.0, using the CC1 estimated rate of $1.954 \times 10^{-7} \pm 2.0152 \times 10^{-8}$ substitutions/site/year obtained with BEAST. “g200” and “g1972” refer to the number of CC1 genomes used in each analyses ($n=200$ and $n=1,972$, respectively). Red lines denote perfect positive correlation coefficients ($R^2=1$).

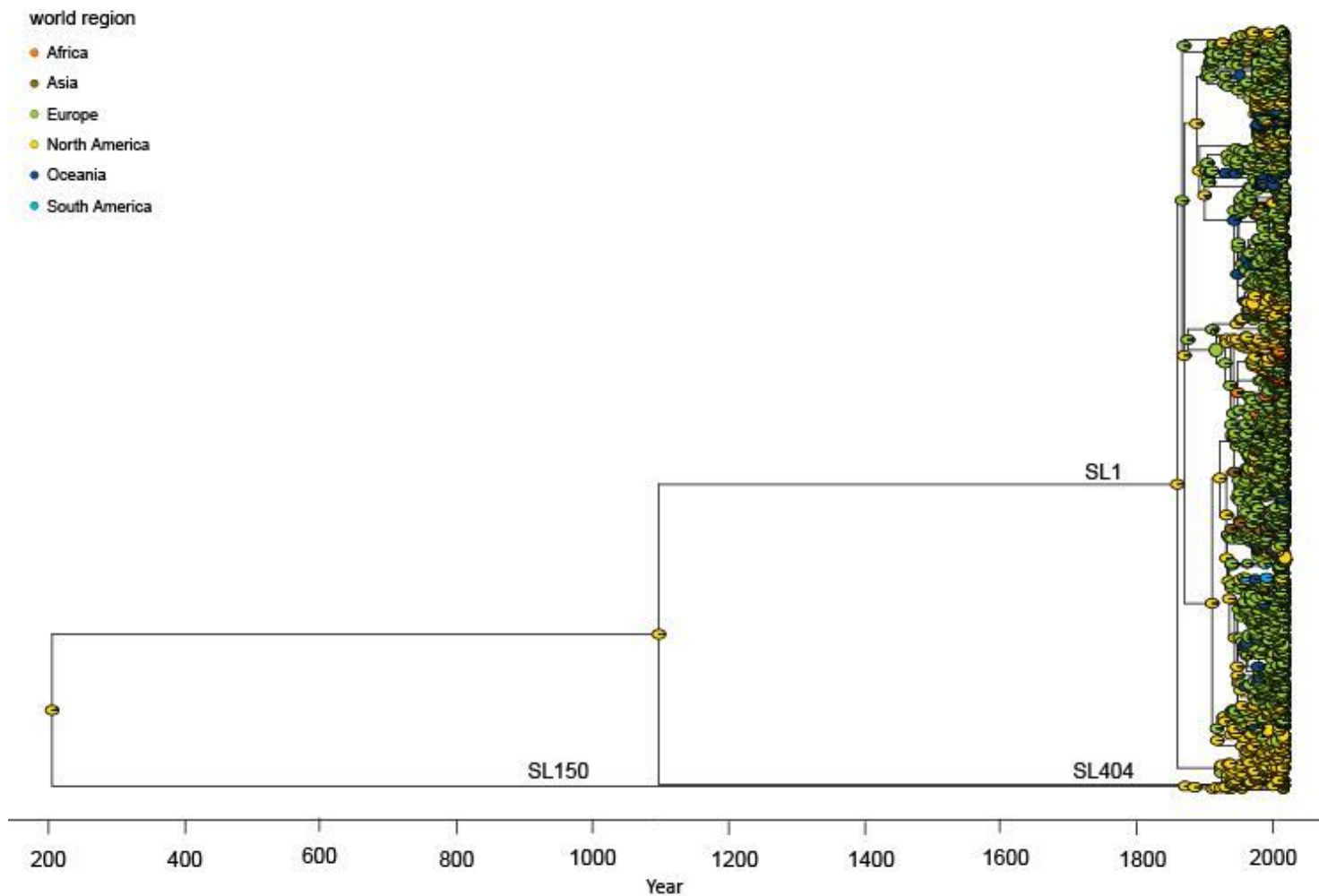


Figure S10. Phylogeography inference of *Lm-CC1* based on 1972 dated genomes.

Pies at the nodes represent the probability of ancestral geographical locations, estimate using PastML using the MPPA method with an F81-like model. The detailed view of SL1 can be found in Figure 3.

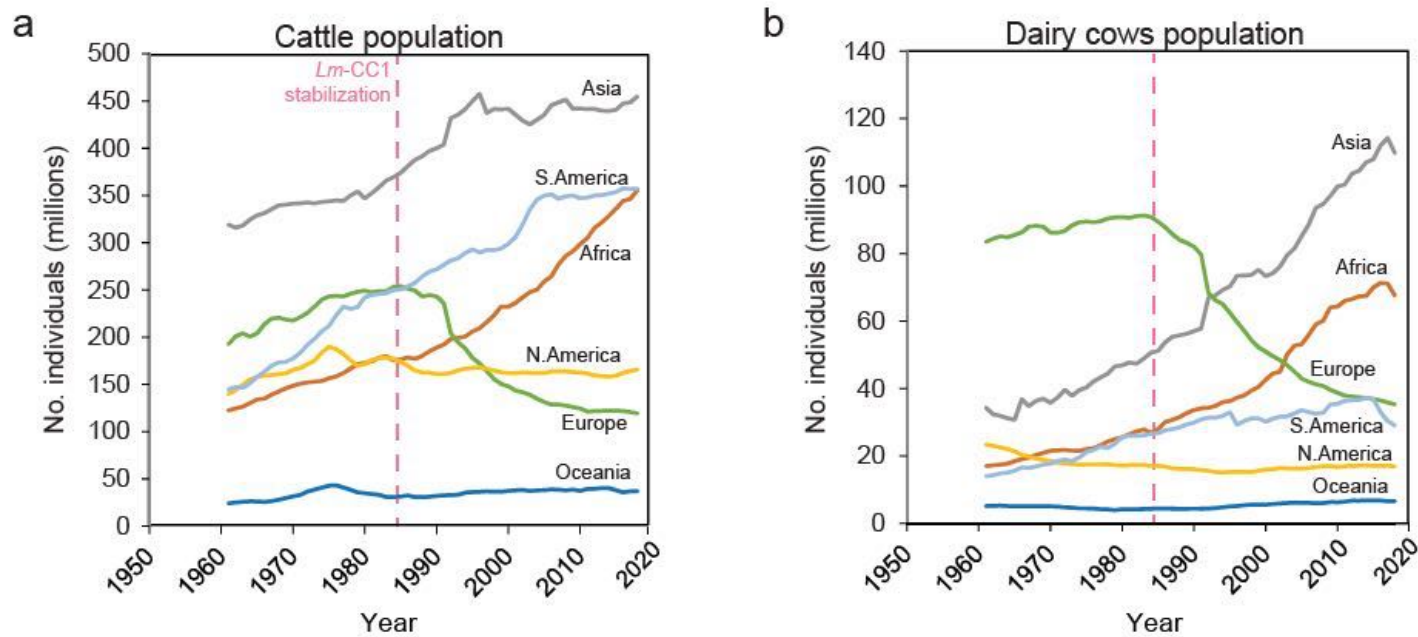


Figure S11. Cattle demographics.

a) Cattle population per world region; b) Dairy cows per world region. Data available for 1961-2018; source: Food and Agriculture Organization of the United Nations; www.fao.org/faostat). Vertical dashed bars mark the estimated date of the stabilization of *Lm-CC1* population size.



Figure S12. French administrative Departments (*départements*). Source: Global Administrative Areas, gadm.org.

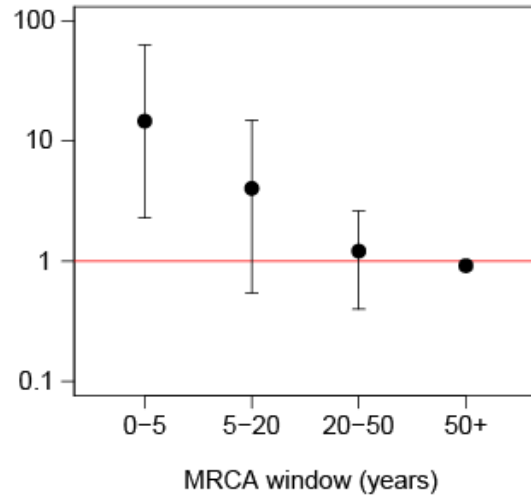


Figure S13. SL1 transmission dynamics within country (France). Relative risk for a pair of isolates to have a MRCA within a defined period when coming from the same Department in France *versus* different ones.

Emergence and global spread of *Listeria monocytogenes* main clinical clonal complex

Alexandra Moura^{1,2,3,*}, Noémie Lefrancq^{4,†}, Alexandre Leclercq^{1,2}, Thierry Wirth^{5,6}, Vítor Borges⁷, Brent Gilpin⁸, Timothy J. Dallman⁹, Joachim Frey¹⁰, Eelco Franz¹¹, Eva M. Nielsen¹², Juno Thomas¹³, Arthur Pightling¹⁴, Benjamin P. Howden¹⁵, Cheryl L. Tarr¹⁶, Peter Gerner-Smidt¹⁶, Simon Cauchemez⁴, Henrik Salje^{4,†,#}, Sylvain Brisse^{17,#}, Marc Lecuit^{1,2,3,18,#,*} for the *Listeria* CC1 Study Group

¹ Institut Pasteur, Biology of Infection Unit, Paris, France

² Institut Pasteur, French National Reference Centre and WHO Collaborating Centre *Listeria*, Paris, France

³ Inserm U1117, Paris, France

⁴ Institut Pasteur, Mathematical Modelling of Infectious Diseases Unit, UMR2000, CNRS, Paris, France.

⁵ Institut Systématique Evolution Biodiversité (ISYEB), Museum National d'Histoire Naturelle, CNRS, Sorbonne Université, Université des Antilles, EPHE, Paris, France

⁶ PSL University, EPHE, Paris, France

⁷ National Institute of Health Dr. Ricardo Jorge, Department of Infectious Diseases, Lisbon, Portugal

⁸ Institute of Environmental Science and Research Limited, Christchurch Science Centre, Christchurch, New Zealand

⁹ Public Health England, London, UK

¹⁰ Vetsuisse, University of Bern, Bern, Switzerland

¹¹ National Institute for Public Health and the Environment (RIVM), Centre for Infectious Disease Control, Bilthoven, Netherland

¹² Statens Serum Institut, Copenhagen, Denmark

¹³ National Institute for Communicable Diseases, Division of the National Health Laboratory Service, Johannesburg, South Africa

¹⁴ Biostatistics and Bioinformatics, Center for Food Safety and Applied Nutrition, U.S. Food and Drug Administration, College Park, MD, United States

¹⁵ Microbiological Diagnostic Unit Public Health Laboratory, Department of Microbiology and Immunology, The Doherty Institute for Infection and Immunity, University of Melbourne, Victoria, Australia; Infectious Diseases Department, Austin Health, Heidelberg, Victoria, Australia

¹⁶ Centers for Disease Control and Prevention, United States

¹⁷ Institut Pasteur, Biodiversity and Epidemiology of Bacterial Pathogens Unit, Paris, France

¹⁸ Université de Paris, Necker-Enfants Malades University Hospital, Division of Infectious Diseases and Tropical Medicine, Institut Imagine, APHP, Paris, France

***Listeria* CC1 Study Group**

Caroline Charlier, Institut Pasteur, French National Reference Center and WHO Collaborating Center *Listeria*, Paris, France; Institut Pasteur, Biology of Infection Unit, Paris-France; Inserm U1117, Paris, France; Université de Paris, Necker-Enfants Malades University Hospital, Department of Infectious Diseases and Tropical Medicine, AP-HP, Paris, France

Guillaume Vales, Institut Pasteur, French National Reference Center and WHO Collaborating Center *Listeria*, Paris, France

Hélène Bracq-Dieye, Institut Pasteur, French National Reference Center and WHO Collaborating Center *Listeria*, Paris, France

Nathalie Tessaud-Rita, Institut Pasteur, French National Reference Center and WHO Collaborating Center *Listeria*, Paris, France

Pierre Thouvenot, Institut Pasteur, French National Reference Center and WHO Collaborating Center *Listeria*, Paris, France

Viviane Chenal-Francois, Institut Pasteur, French National Reference Center and WHO Collaborating Center *Listeria*, Paris, France

Zuzana Kucerova, Centers for Disease Control and Prevention, Atlanta, Georgia, United States

Heather Carleton, Centers for Disease Control and Prevention, Atlanta, Georgia, United States

Steven Stroika, Centers for Disease Control and Prevention, Atlanta, Georgia, United States

Anders Gonçalves da Silva, Microbiological Diagnostic Unit Public Health Laboratory, Department of Microbiology and Immunology, The Doherty Institute for Infection and Immunity, University of Melbourne, Victoria, Australia

Karolina Mercoulia, Microbiological Diagnostic Unit Public Health Laboratory, Department of Microbiology and Immunology, The Doherty Institute for Infection and Immunity, University of Melbourne, Victoria, Australia

Anthony Marius Smith, National Institute for Communicable Diseases, Division of the National Health Laboratory Service, Johannesburg, South Africa.

Jonas T. Björkman, Statens Serum Institut, Copenhagen, Denmark

Anna Oevermann, Division of Neurological Diseases, DCR-VPH, Vetsuisse Faculty, University of Bern, Bern, Switzerland

Lisandra Aguillar-Bultet, Vetsuisse Faculty, University of Bern, Bern, Switzerland

Thijs Bosch, National Institute for Public Health and the Environment (RIVM), Centre for Infectious Disease Control, Bilthoven, Netherland

Sjoerd Kuiling, National Institute for Public Health and the Environment (RIVM), Centre for Infectious Disease Control, Bilthoven, Netherland

Maaïke van den Beld, National Institute for Public Health and the Environment (RIVM), Centre for Infectious Disease Control, Bilthoven, Netherland

Anaïs Passet, Public Health England, London, United Kingdom

Kathie Grant, Public Health England, London, United Kingdom

Leonor Silveira, National Institute of Health Dr. Ricardo Jorge, Department of Infectious Diseases, Lisbon, Portugal

Ângela Pista, National Institute of Health Dr. Ricardo Jorge, Department of Infectious Diseases, Lisbon, Portugal

Mónica Oleastro, National Institute of Health Dr. Ricardo Jorge, Department of Infectious Diseases, Lisbon, Portugal

Sven Halbedel, Consultant Laboratory for *Listeria monocytogenes*, FG11, Robert Koch Institute, Wernigerode, Germany